

POLITECNICO DI TORINO

MASTER THESIS

---

Combustion CFD modeling in  
CNG/H<sub>2</sub> fueled IC engines by  
means of a LFS flame  
surface-density model

---



*Author:*  
Moein AMIRMOSTOFIAN

*Supervisor:*  
Daniela MISUL  
Mirko BARATTA

*A thesis submitted for the degree of Master of Science in  
Mechanical Engineering*

*in the*

Department of Mechanical and Aerospace Engineering

July 18, 2018



# *Abstract*

## **Combustion CFD modeling in CNG/H<sub>2</sub> fueled IC engines by means of a LFS flame surface-density model**

by Moein AMIRMOSTOFIAN

A significant proportion of our daily routine has always been spent traveling from one place to another place. Fossil fuel, particularly petroleum fuel, consumption is steadily rising as a result of population growth which in parallel raises the concerns over the possible environmental issues such as greenhouse gases (GHG) emissions released to the atmosphere that contribute to acid rains and global warming.

In order to protect our planet from major environmental challenges that we are likely to face later in this century, some international coordinated efforts have been adopted in order to tackle climate changes. In Paris, on 12 December 2015, 196 Parties to the United Nations Framework Convention on Climate Change (UNFCCC) reached a landmark agreement so-called The Paris Agreement to combat climate change which describes the gravity of this issue.

Inevitably the growth of population causes a simultaneous increment in human mobility requirement that leads to the widespread presence of internal combustion (IC) engine which is the power source and mechanical heart sustaining the concept of contemporary mobility.

To this issue, automotive sectors made a crucial effort and devoted to a strict decarbonization process to push the European transport sector to the 2050 target and the use of Low Carbon Alternative Fuels, like Compressed Natural Gas, will play a fundamental role to quicken this process.

Natural gas (CNG) is considered as an alternative vehicle fuel because of its economic and environmental advantages which is a clean fuel with CH<sub>4</sub> as its major component which produces 20% less CO<sub>2</sub> than the other conventional fuel such as gasoline, that is considered to be one of the most favorable fuels for engines. However, due to the slow-burning velocity of CNG and its poor lean-burn capability, the CNG spark-ignition engine still has some disadvantages like low thermal efficiency, large cycle-by-cycle variation, and these decrease engine power output and increase fuel consumption.

To improve the lean-burn capability and flame burning velocity of natural gas, one effective method to solve the problem is to blend natural gas with fuel that possesses fast burning velocity engines under lean-burn conditions. Hydrogen is regarded as the best gaseous candidate for natural gas due to its very fast burning velocity and this combination is expected to improve lean-burn characteristics and decrease engine emissions.

Alongside the type of fuel which is crucially decisive, there is an effective technique so-called EGR used in IC engines to reduce pollution, specifically to control NO<sub>x</sub> emissions. However, as the EGR rate at a given engine operating condition rises, the combustion instability increases which produce cyclic variations resulting in the deterioration of engine performance. Therefore, the optimum EGR rate should be carefully determined in order to obtain the better engine performance and emissions. To this aim, the thesis has been conducted to investigate the combustion stability and engine performance for pure CH<sub>4</sub> and also CNG blended with different percentages of hydrogen, based on the variation of Indicated Mean Effective Pressure (CoV imep) and MFB50.

This work is a consequence of collaboration with engine's research team at Polytechnic University of Turin composed of master and Ph.D. students, led by professors D. Misul and M. Baratta.



## *Acknowledgements*

I would like to express my great gratitude to my supervisors Prof. Daniela Misul and Prof. Mirko Bratta for the useful comments, remarks, patience, and the permanent support through the learning process of this master thesis. Furthermore, I would like to thank Prashant Goel, the Ph.D. student of this sector, for introducing me to the topic as well for the support on the way. Also, I like to thank Fabio Zardini, my colleague, for his participation and comments.

Lastly, I would like to thank my loved ones, who have supported me throughout the entire process, both by keeping me harmonious and helping me putting pieces together.



# Contents

<b>Abstract</b>	<b>iii</b>
<b>Acknowledgements</b>	<b>v</b>
<b>1 CFD Analysis - Introduction</b>	<b>1</b>
1.1 Basic equations of Fluid Flow, Navier-Stokes equation . . . . .	2
1.1.1 Navier-Stokes Equation for Compressible Flow . . . . .	5
1.2 Finite Volume method . . . . .	6
1.2.1 Solution procedure . . . . .	7
1.3 Turbulent flow . . . . .	7
1.3.1 The k- $\epsilon$ Turbulence Model . . . . .	9
1.4 Mesh Generation . . . . .	11
1.4.1 Grid Scaling . . . . .	11
1.4.2 Fixed Embedding . . . . .	11
1.4.3 Adaptive Mesh refinement . . . . .	12
<b>2 Natural Gas — Why is Methane a Clean Fuel?</b>	<b>15</b>
2.1 Introduction To Methane . . . . .	15
2.2 Clean Combustion . . . . .	15
2.3 The Age of Methane . . . . .	16
2.4 Global Dynamics . . . . .	17
<b>3 The Effect of Air-Fuel Ratio (<math>\lambda</math>) on Combustion</b>	<b>19</b>
3.1 Stoichiometric Combustion Reaction . . . . .	19
3.2 Air-Fuel Ratio . . . . .	19
3.2.1 Stoichiometric Air-Fuel Ratio . . . . .	20
3.2.2 Air-fuel ratio equivalence factor – $\lambda$ . . . . .	20
3.3 How does the air-fuel ratio affect the engine performance? . . . . .	21
<b>4 Turbulent Length Scales</b>	<b>23</b>
4.1 introduction . . . . .	23
4.2 Kolmogorov length scale . . . . .	23
4.3 Internal Length Scale . . . . .	24
4.4 Energy Transfer . . . . .	24
4.4.1 Energy Spectrum . . . . .	25
4.4.2 Full Spectrum . . . . .	25
4.5 Procedure . . . . .	25
4.5.1 Polito Engine Figures . . . . .	26
4.5.2 GasOn Figures . . . . .	28
4.5.3 Polito Engine VS GasOn . . . . .	30
4.5.4 Ensembling . . . . .	30
Polito Engine . . . . .	31
GasOn . . . . .	32

	Ensembling (Polito Engine) . . . . .	34
	Ensembling (GasOn) . . . . .	35
	Ensembling (Polito Engine VS GasOn) . . . . .	36
4.6	Mesh Independency . . . . .	37
4.7	Conclusion . . . . .	39
<b>5</b>	<b>Laminar Flame Speed</b>	<b>41</b>
5.1	Laminar Premixed Flame . . . . .	41
5.1.1	Governing equations . . . . .	44
5.2	Methods to predict Laminar flame speed . . . . .	45
5.3	Gulder vs LFS table . . . . .	46
5.3.1	Reliability . . . . .	46
5.3.2	Conclusion . . . . .	50
5.4	The Effect of EGR on Gulder and LFStable Models . . . . .	51
5.4.1	Introduction to Exhaust Gas Recirculation (EGR) . . . . .	51
5.4.2	Procedure . . . . .	52
	EGR effect on Gulder and LFStable models . . . . .	52
5.4.3	Conclusion . . . . .	53
<b>6</b>	<b>Use of Hydrogen-Methane Blends in Internal Combustion Engines</b>	<b>55</b>
6.1	Introduction . . . . .	55
6.2	Procedure . . . . .	56
	HCNG15% $\lambda = 1.0$ . . . . .	57
	HCNG25% $\lambda = 1.0$ . . . . .	58
	HCNG15% $\lambda = 1.4$ . . . . .	59
	Re-calibration HCNG15% $\lambda = 1.4$ . . . . .	60
	HCNG25% $\lambda = 1.4$ . . . . .	61
	Re-calibration HCNG25% $\lambda = 1.4$ . . . . .	62

# List of Figures

1.1	CFD Steps . . . . .	1
1.2	Convection of a Disturbance in a Pipe . . . . .	4
1.3	Diffusion in a Pipe . . . . .	4
1.4	Convection and Diffusion in a Pipe . . . . .	4
1.5	Sample three-cell, One-dimensional spatial domain [10] . . . . .	6
1.6	Solution Order of the Transport Equation. The Turbulence Equation were removed from the PISO loop for efficiency reasons.	7
1.7	Evolution of a combusting spray bomb. This grid was generated by AMR (a) 0.5, (b)1.0, and (c)2.0 milliseconds after the start of the simulation. the left column shows the grid only, while he right column shows the grid and temperature values (black represents a temperature of approximately 2800K) for corresponding times. This case has an ambient temperature of 1000 K,an ambient density of $14.8 \text{ kg/m}^3$ , an orifice diameter of 0.180mm, and an injection pressure of 136 Mpa . . . . .	13
2.1	History of energy consumption in US (1776-2012)[11] . . . . .	16
3.1	Engine power and fuel consumption as a function of air-fuel ratio ( $\lambda$ ) for Gasoline[9] . . . . .	21
4.1	Turbulent flow composed of multi-sized eddies[17] . . . . .	23
4.2	Different length scales and ranges in turbulence energy cascade[18]	24
4.3	Eney spectrum of turbulent flow[18] . . . . .	25
5.1	Schematic of Bunsen Burner[6] . . . . .	41
5.2	Kinematic balance for a steady oblique flame[6] . . . . .	42
5.3	Laminar spherical flame propagation in a combustion bomb . .	43
5.4	Flame structure of laminar lean flame [6] . . . . .	44
5.5	Burning velocities calculated with a starting C1-Mechanism and a starting C2-mechanism, several data compiled by Warnatz[14] and recent data referenced by Law[15] for atmospheric methane-air flames . . . . .	45
5.6	The base calibration for both models . . . . .	47
5.7	Gulder model re-calibration . . . . .	48
5.8	Gulder model re-calibration . . . . .	49
5.9	Gulder model re-calibration . . . . .	49
5.10	Gulder model re-calibration . . . . .	50
5.11	Gulder model re-calibration . . . . .	50
5.12	Exhaust gas recirculation[7] . . . . .	51
5.13	Differential pressure at different EGR valve opening level (1600rpm, 190 Nm)[16] . . . . .	52
5.14	LFStable model $\lambda = 1.0$ . . . . .	53
5.15	Gulder model model $\lambda = 1.0$ . . . . .	53

6.1	Burning velocities and flame speed for different percentages of hydrogen in methane ( $\varphi = 1.0$ )[5]	56
6.2	Wrinkling factor=20 $\alpha=1.8$	59
6.3	Wrinkling factor=20 $\alpha=1.8$	59
6.4	Wrinkling factor=30 $\alpha=1.8$	60
6.5	Wrinkling factor=30 $\alpha=1.8$	60
6.6	Wrinkling factor=20 $\alpha=1.8$	61
6.7	Wrinkling factor=20 $\alpha=1.8$	61
6.8	Wrinkling factor=35 $\alpha=2.1$	62
6.9	Wrinkling factor=35 $\alpha=2.1$	62

# List of Tables

3.1	the stoichiometric air-fuel ratio for some fossil fuels[12]	20
3.2	Types of combustible mixtures[12]	21
4.1	630° Crank angle degree (CAD)	39
6.1	Overall comparison of properties of hydrogen, CNG, HCNG and gasoline[2]	55
6.2	Properties of CNG and HCNG blends with different hydrogen content[3]	56



## Chapter 1

# CFD Analysis - Introduction

Computational Fluid Dynamics (CFD) is the branch of fluid dynamics providing a cost effective means of simulating real flows by the numerical solution of the governing equations. The governing equations for Newtonian fluids, namely Navier-Stokes equations, have been known for over 150 years. However, the development of reduced forms of these equation is still an active area of research, in particular, the turbulent closure of the Reynolds-averaged Navier-Stokes equations. For non-Newtonian fluids, chemically reacting flows and two phase flows, the theoretical development is at less advanced stage (Sayma, 2009). Experimental methods have played an important role in validating and exploring the limits of the various approximations to the governing equations, particularly wind tunnel and rig tests that provide a cost effective alternative to full scale testing. The flow governing equations are extremely complicated such that analytic solutions cannot be obtained for most practical applications. Computational techniques replace the governing partial differential equations with systems of algebraic equations that are much easier to solve using computers. The steady improvement in computing power, since the 1950's, thus has led to emergence of CFD. This branch of fluid dynamics complements experimental and theoretical fluid dynamics by providing alternative potentially cheaper means of testing fluid flow systems. It also can allow for the testing of conditions which are not possible or extremely difficult to measure experimentally and are not amenable to analytic solutions (Sayma, 2009).

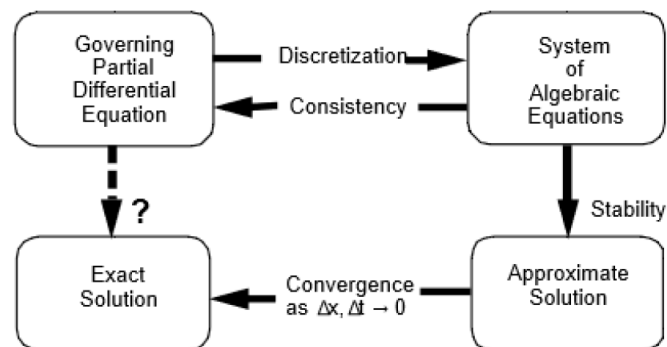


**Figure 1.1:** CFD Steps

CFD techniques have so emerged with the advent of digital computers. Since then, a large number of numerical methods were developed to solve flow problems using this approach. The purpose of a simulation is to find out how the flows behave in a given system for a given set of inlet and outlet conditions.

The so called boundary conditions.

The basic concept of CFD methods is to find the values of a flow quantities in at a large number of points of the system. These points are usually connected together in what is called numerical grid or mesh. The system of differential equations representing the flow is converted, using some procedure, to a system of algebraic equations representing the inter dependency of the flow at those points and their neighbouring points. The resulting system of algebraic equations, which can be linear or non-linear, is usually large and requires a digital computer to solve. So in a CFD problem there will be a system with the unknowns being the flow quantities at the mesh points. Solution of this system results in the knowledge of these quantities at mesh points. If the flow is unsteady, either due to varying boundary conditions, or due to inherent unsteadiness, the solution procedure is repeated at discrete time intervals to predict the evolution in time of the flow variables.

With the development of fast and validated numerical procures, and the continuous increase in computer speed and availability of cheap memory, larger and larger problems are being solved using CFD methods at cheaper cost and quicker turnaround times. In many design and analysis applications, CFD methods are quickly replacing experimental and analytical methods.

It should be noted that there are certain levels of numerical approximations and assumptions made during the development of CFD models. Hence, good understanding of the applicability range and the limitations of a CFD tools is essential to enable the correct use of these tools.

In additions to the speed and reduced cost of CFD methods, compared to experimental procedures in most engineering applications, they also offer a more complete set of information. They usually provide all relevant flow information throughout the domain of interest. Experimental methods are mostly limited to measurements of some flow quantities at certain locations accessible by the measuring equipment.

CFD simulations also enable flow solutions at the true scale of the engineering systems with the actual operating conditions, while experimental measurements mostly require either scaling up or down. In most cases realistic conditions cannot be economically represented and thus results need to be extrapolated; this problem does not exist in CFD simulations.

In automotive applications CFD is nowadays used in a large number of areas including engine components but also auxiliary systems and for modelling the aerodynamics of the car to minimize drag and optimize the down force under various operating conditions.

## 1.1 Basic equations of Fluid Flow, Navier-Stokes equation

Fluid flow equations are made essentially of differential equations representing the interrelationship between the flow variables and their evolution in time and in space. These equations are complemented by algebraic relations such as the equation of state for compressible flow.

The Navier-Stokes and continuity equations provide the foundations for modelling fluid motion. The laws of motion that apply to solids are valid for all matter including liquids and gases. A principal difference, however, between

fluids and solids is that fluids distort without limit. For example, if a shear stress is applied to a fluid, then layers of the fluid particles will move relative to each other and the particles will not return to their original position if application of the shear force is stopped. Analysis of a fluid needs to take account of such distortions.

A fluid particle responds to a force in the same way that a solid particle will. If a force is applied to a particle, acceleration will result as governed by Newton's second law of motion, which states that the rate of change of momentum of a body is proportional to the unbalanced force acting on it and takes place in the direction of the force. It is useful to consider the forces that a fluid particle can experience. These include:

- Body forces such as gravity and electromagnetism
- Force due to pressure
- Force due to viscous action
- Forces due to rotation

Assuming that the shear rate in a fluid is linearly related to shear stress, and that the fluid flow is laminar, Navier (1823) derived the equations of motion for a viscous fluid from molecular considerations. Stokes (1845) also derived the equations of motion for a viscous fluid in a slightly different form and the basic equations that govern fluid flow are now generally known as the Navier-Stokes equations of motion. The Navier-Stokes equations can also be used for turbulent flow, with appropriate modifications. The Navier-Stokes equations can be derived by considering the dynamic equilibrium of a fluid element.

Taking for example the temperature distribution of a flow in a straight pipe, where the velocity is fixed by pumping a fixed volume flow rate into the pipe. Assume also that the flow velocity is not altered by the change in temperature. The temperature distribution  $T(x,t)$  in the pipe as a function of the pipe axial coordinate  $x$  is given by the following differential equation:

$$\frac{\partial T}{\partial t} + u \frac{\partial T}{\partial x} - \alpha \frac{\partial^2 T}{\partial x^2} = 0 \quad (1.1)$$

Where  $u$  is the flow velocity which is assumed constant across the pipe,  $t$  is time and  $\alpha$  is the thermal diffusivity. In the above equation the first term is the time derivative expressing the temperature gradient with time. The second term is called the advection term which is responsible for the transport of any temperature disturbance with the flow without any distortion. The third term is called the diffusion term, which is responsible for the spread of any disturbance in all directions.

If the thermal diffusivity is assumed to be negligible equation 1.1 reduces to:

$$\frac{\partial T}{\partial t} + u \frac{\partial T}{\partial x} = 0 \quad (1.2)$$

A temperature disturbance entering the pipe from the left at time  $t=0$  will be convected without any distortion after a while to the right. If the velocity is zero equation 1.1 reduce to:

$$\frac{\partial T}{\partial t} - \alpha \frac{\partial^2 T}{\partial x^2} = 0 \quad (1.3)$$

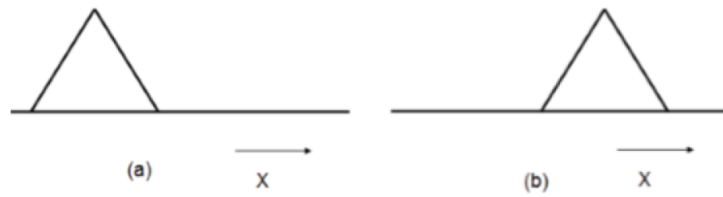


**Figure 1.2:** Convection of a Disturbance in a Pipe

A temperature disturbance shown in in the above figure will be diffused to the right and left and reduced in amplitude after a while.

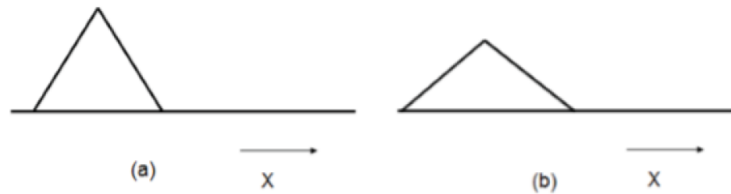


**Figure 1.3:** Diffusion in a Pipe

The action of both convection and diffusion can now be added together to represent the behavior of described by equation int1 where a disturbance introduced at the left, will both be convected and diffused (Fig:diffu).

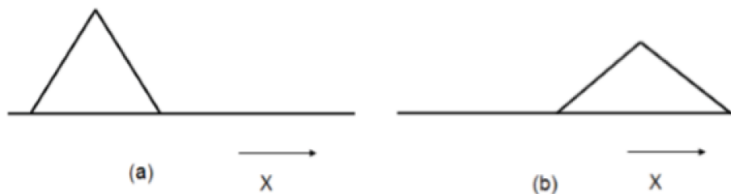


**Figure 1.4:** Convection and Diffusion in a Pipe

The simplicity of this system enabled a straightforward interpretation of various terms. Equation 1.1 is said to be linear because the velocity is assumed constant and does not depend on temperature. Hence there is only one dependent variable, which is the temperature. A system which might include a non-linear convective term is shown in the equation below:

$$\frac{\partial u}{\partial t} + u \frac{\partial u}{\partial x} - \alpha \frac{\partial^2 u}{\partial x^2} = 0 \quad (1.4)$$

This equation represents the transport of momentum along the pipe. In this case, velocity is the dependent variable and it is not assumed to be constant. The non-linearity arises in the convective term where the velocity, which is the sought variable, is being convected by the action of the velocity itself.

### 1.1.1 Navier-Stokes Equation for Compressible Flow

Once the Navier-Stokes equations are derived those could be arranged in a simplified form for both compressible or incompressible fluid flow. In this section the equations for Compressible fluid flows will be analyzed.

The flow governing equations are the continuity equation, momentum equation (Navier- Stokes) and energy equation.

The continuity equation:

$$-\frac{\partial \rho}{\partial t} = \frac{\partial(\rho u)}{\partial x} + \frac{\partial(\rho v)}{\partial y} + \frac{\partial(\rho w)}{\partial z} \quad (1.5)$$

The Navier-Stokes equation:

$$\rho \left( \frac{\partial u}{\partial t} + u \frac{\partial u}{\partial x} + v \frac{\partial u}{\partial y} + w \frac{\partial u}{\partial z} \right) = -\frac{\partial p}{\partial x} + \mu \left( \frac{\partial^2 u}{\partial x^2} + \frac{\partial^2 u}{\partial y^2} + \frac{\partial^2 u}{\partial z^2} \right) + F_x \quad (1.6)$$

$$\rho \left( \frac{\partial v}{\partial t} + u \frac{\partial v}{\partial x} + v \frac{\partial v}{\partial y} + w \frac{\partial v}{\partial z} \right) = -\frac{\partial p}{\partial y} + \mu \left( \frac{\partial^2 v}{\partial x^2} + \frac{\partial^2 v}{\partial y^2} + \frac{\partial^2 v}{\partial z^2} \right) + F_y \quad (1.7)$$

$$\rho \left( \frac{\partial w}{\partial t} + u \frac{\partial w}{\partial x} + v \frac{\partial w}{\partial y} + w \frac{\partial w}{\partial z} \right) = -\frac{\partial p}{\partial z} + \mu \left( \frac{\partial^2 w}{\partial x^2} + \frac{\partial^2 w}{\partial y^2} + \frac{\partial^2 w}{\partial z^2} \right) + F_z \quad (1.8)$$

$$\rho c_p \left( \frac{\partial T}{\partial t} + u \frac{\partial T}{\partial x} + v \frac{\partial T}{\partial y} + w \frac{\partial T}{\partial z} \right) = \phi + \frac{\partial}{\partial x} \left( k \frac{\partial T}{\partial x} \right) + \frac{\partial}{\partial y} \left( k \frac{\partial T}{\partial y} \right) + \frac{\partial}{\partial z} \left( k \frac{\partial T}{\partial z} \right) + \left( u \frac{\partial p}{\partial x} + v \frac{\partial p}{\partial y} + w \frac{\partial p}{\partial z} \right) \quad (1.9)$$

Where  $\phi$  is the dissipation function,  $u, v, w$  are the velocity components in the  $x, y, z$  directions,  $\rho$  is the density,  $T$  is the temperature,  $p$  is the pressure,  $\mu$  is the viscosity and  $c_p$  is the specific heat at constant pressure.

The continuity equation is an expression representing the mass conservation law; per unit volume, the sum of all masses flowing in and out per unit time must be equal to the change of the mass due to change in density per unit time.

The continuity equation applies to all fluids, compressible and in-compressible flow, Newtonian and non-Newtonian fluids. It expresses the law of conservation of mass at each point in a fluid and must therefore be satisfied at every point in a flow field. It is worthwhile to offer brief comment on the physical significance of equations (1.6-1.8). The terms on the left side are often referred to as inertial terms, and arise from the momentum changes. These are countered by the pressure gradient,  $\partial p / \partial x$ , viscous forces which always act to retard the flow, and if present, body forces. The inertial term gives a measure of the change of velocity of one fluid element as it moves about in space. The term  $\partial / \partial t$  gives a measure of the change of velocity at a fixed point and it known as the local derivative. The remaining three terms of the inertial term are grouped together and known as the convective terms or convective differential.

Assuming constant properties of viscosity and specific heat, the above system of equations contains six unknowns. With only five equations available, a further equation is needed to close the system. Usually this is provided by a constitutive relation for the pressure. For example, for an ideal gas, the

relation between temperature and pressure is given by  $p = \rho RT$ , where  $R$  is the gas constant.

## 1.2 Finite Volume method

Finite volume methods can be used to numerically solve the integral form of the conservation equations. An advantage of the finite volume method is that it conserves transported quantities for regularly or irregularly shaped cells. To understand the inputs for finite volume, consider the simple three cell computational domain shown below in Figure

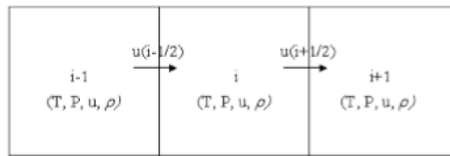


**Figure 1.5:** Sample three-cell, One-dimensional spatial domain [10]

Now consider the simple transport equation

$$\frac{\partial \phi}{\partial t} + \frac{\partial u\phi}{\partial x} = 0 \quad (1.10)$$

The above equation can be written in integral form as

$$\frac{d}{dt} \int_V \phi dV + \int_S u * n\phi dS = 0 \quad (1.11)$$

Where  $V$  is the cell volume,  $S$  is the surface area, and  $n$  is the surface normal. As discussed earlier, finite volume methods solve the integral form of the conservation equations instead of the differential form. The integral form of the equation is solved by summing fluxes on the faces of the cells. Usually all values are collocated and stored at the center of the cell as shown in Figure 1.5. Thus, to solve the integral form of the equation, the velocity and  $f$  must be interpolated to the cell surface. There are several options for obtaining the cell surface value. One option is to average the two adjacent cell values and place them on the surface, which results in a surface  $f$  given as

$$\phi_{i+1/2} = \frac{1}{2}\phi_i + \frac{1}{2}\phi_{i+1} \quad (1.12)$$

$$\phi_{i-1/2} = \frac{1}{2}\phi_i + \frac{1}{2}\phi_{i-1} \quad (1.13)$$

Another option is to upwind the surface value for  $f$ , which results in

$$\phi_{i+1/2} = \phi_i \quad (1.14)$$

$$\phi_{i-1/2} = \phi_{i-1} \quad (1.15)$$

### 1.2.1 Solution procedure

Understanding the order in which the transport equations are solved is important for appropriately configuring your simulation parameters.



**Figure 1.6:** Solution Order of the Transport Equation. The Turbulence Equation were removed from the PISO loop for efficiency reasons.

At the start of each time-step, the previous values (the time-step minus 1) are stored for all transported quantities. Next, explicit sources are calculated for each sub model that is currently activated and radiation is solved if energy and radiation are decoupled. At this time the PISO loop begins. At the beginning of the PISO loop (i.e., the first PISO iteration), CONVERGE solves for momentum and pressure, which sets the velocity for the other transport equations. After each PISO iteration, it is necessary to check for PISO loop Convergence [10].

## 1.3 Turbulent flow

There are two radically different states of flows that are easily identified and distinguished: laminar flow and turbulent flow. Laminar flows are characterized by smoothly varying velocity fields in space and time in which individual "laminar" (sheets) move past one another without generating cross currents. These flows arise when the fluid viscosity is sufficiently large to damp out any perturbations to the flow that may occur due to boundary imperfections or other irregularities. These flows occur when at low-to-moderate values of the

Reynolds number.

In contrast, turbulent flows are characterized by large, nearly random fluctuations in velocity and pressure in both space and time. These fluctuations arise from instabilities that grow until nonlinear interactions cause them to break down into finer and finer whirls that eventually are dissipated (into heat) by the action of viscosity. Turbulent flows occur in the opposite limit of high Reynolds numbers.

The equations governing a turbulent flow are precisely the same as for a laminar flow, however, the solution is clearly much more complicated in this regime. The approaches to solving the flow equations for a turbulent flow field can be roughly divided into two classes. Direct Numerical Simulations (DNS) use the speed of modern computers to numerically integrate the Navier-Stokes equations, resolving all of the spatial and temporal fluctuations, without resorting to modelling. In essence, the solution procedure is the same as for laminar flow, except the numerics must contend with resolving all of the fluctuations in the velocity and pressure. DNS remains limited to very simple geometries (e.g., channel flows, jets and boundary layers) and is extremely expensive to run.

The alternative to DNS found in most CFD packages (including STAR®) is to solve the Reynolds Averaged Navier Stokes (RANS) equations or, less widespread, the Large Eddy Simulation (LES) which takes in account the energy of the largest eddy. RANS equations govern the mean velocity and pressure. Because these quantities vary smoothly in space and time, they are much easier to solve; however, as will be shown below, they require modelling to “close” the equations and these models introduce significant error into the calculation. To demonstrate the closure problem, we consider fully developed turbulent flow in a channel of height  $2H$ . Recall that with RANS we are interested in solving for the mean velocity  $\bar{u}(y)$  only.

If we formally average the Navier-Stokes equations and simplify for this geometry, we arrive at the following

$$\frac{\partial \overline{u'v'}}{\partial y} + \frac{1}{\rho} \frac{\partial \bar{p}}{\partial y} = \frac{\partial^2 \bar{u}(y)}{y^2} \quad (1.16)$$

Subject to the boundary condition

$$\frac{\partial \bar{u}}{\partial y} = 0 \quad \text{for } y = 0 \quad (1.17)$$

$$\bar{u} = 0 \quad \text{for } y = H \quad (1.18)$$

The quantity  $\overline{u'v'}$  called Reynolds stress, is a higher-order moment that must be modeled in terms of the knowns (i.e.,  $\bar{u}(y)$  and its derivatives). This is referred to as the “closure” approximation. The quality of the modelling of this term will determine the reliability of the computations. Turbulence modelling is a rather broad discipline and an in-depth discussion is beyond the scope of this introduction. Here we simply note that the Reynolds stress is modelled in terms of two turbulence parameters, the turbulent kinetic energy  $k$  and the turbulent energy dissipation rate  $\epsilon$  defined below. This method is usually known as  $k$ - $\epsilon$  method.

$$k = \frac{1}{2}(\overline{u'^2} + \overline{v'^2} + \overline{z'^2}) \quad (1.19)$$

$$\epsilon = v \left[ \left( \frac{\partial u'}{\partial x} \right)^2 + \left( \frac{\partial u'}{\partial y} \right)^2 + \left( \frac{\partial u'}{\partial z} \right)^2 + \left( \frac{\partial v'}{\partial x} \right)^2 + \left( \frac{\partial v'}{\partial y} \right)^2 + \left( \frac{\partial v'}{\partial z} \right)^2 + \left( \frac{\partial w'}{\partial x} \right)^2 + \left( \frac{\partial w'}{\partial y} \right)^2 + \left( \frac{\partial w'}{\partial z} \right)^2 \right] \quad (1.20)$$

Where  $(u, v, w')$  is the fluctuating velocity vector. The kinetic energy is zero for laminar flow and can be as large as 5 % of the kinetic energy of the mean flow in a highly turbulent case.

The family of models is generally known as  $k$ - $\epsilon$  and they form the basis of most CFD packages.

### 1.3.1 The $k$ - $\epsilon$ Turbulence Model

Traditionally, RANS models use an effective turbulent viscosity to model the Reynolds stress term. Thus, additional turbulent diffusion (i.e., diffusive mixing) models the turbulent convective mixing. The modeled Reynolds stress for the Standard  $k$ - $\epsilon$  and RNG models is given by

$$\tau_{ij} = -\bar{\rho} \widetilde{u'_i u'_j} = 2\mu_t S_{ij} - \frac{2}{3} \delta_{ij} \left( \rho k + \mu_t \frac{\partial \widetilde{u'_i}}{\partial x_i} \right) \quad (1.21)$$

The turbulent kinetic energy,  $k$ , is defined as half of the trace of the stress tensor:

$$k = \frac{1}{2} \widetilde{u'_i u'_i} \quad (1.22)$$

Where the turbulent viscosity,  $\mu_t$  is given by

$$\mu_t = c_\mu \rho \frac{k^2}{\epsilon} \quad (1.23)$$

In the previous equation,  $c_\mu$  is a model constant that can be tuned for a particular flow and  $\epsilon$  is the dissipation of turbulent kinetic energy. The mean strain rate tensor  $S_{ij}$  is given by

$$S_{ij} = \frac{1}{2} \left( \frac{\partial \widetilde{u'_i}}{\partial x_j} + \frac{\partial \widetilde{u'_j}}{\partial x_i} \right) \quad (1.24)$$

The models use turbulent diffusion and turbulent conductivity terms to account for the presence of turbulence in mass transport and energy transport. The turbulent diffusion and conductivity terms are given by

$$D_t = \left( \frac{1}{Sc_t} \right) \mu_t \quad (1.25)$$

$$K_t = \left( \frac{1}{Pr_t} \right) \mu_t c_p \quad (1.26)$$

where  $Sc_t$  is the turbulent Schmidt number,  $Pr_t$  is the turbulent Prandtl number,  $D_t$  is the turbulent diffusion, and  $K_t$  is the turbulent conductivity. For the standard  $k$ - $\epsilon$  and RNG  $k$ - $\epsilon$  models, additional transport equations are

needed to obtain the turbulent viscosity given by equation 1.22. One equation is needed for the turbulent kinetic energy,  $k$ , and one for the dissipation of turbulent kinetic energy,  $\epsilon$ . The turbulent kinetic energy transport equation is given by

$$\frac{\partial \rho \epsilon}{\partial t} + \frac{\partial \rho u_i k}{\partial x_i} = \tau_{ij} \frac{\partial u_i}{\partial x_j} + \frac{\partial}{\partial x_j} \frac{\mu}{Pr_k} \frac{\partial k}{\partial x_j} - \rho \epsilon + \frac{c_s}{1.5} S_s \quad (1.27)$$

In the previous equation, the factor of 1.5 is an empirical constant. The transport equation for the dissipation of turbulent kinetic energy is given by

$$\frac{\partial \rho \epsilon}{\partial t} + \frac{\partial \rho u_i \epsilon}{\partial x_i} = \frac{\partial}{\partial x_i} \left( \frac{\mu}{Pr_k} \frac{\partial \epsilon}{\partial x_j} \right) + c_{\epsilon 3} \rho \epsilon \frac{\partial u_i}{\partial x_i} + \left( c_{\epsilon 1} \frac{\partial u_i}{\partial x_j} \tau_{ij} - c_{\epsilon 2} \rho \epsilon + c_s S_s \right) \frac{\epsilon}{k} + S - \rho R \quad (1.28)$$

where  $S$  is the user-supplied source term and  $S_s$  is the source term that represents interactions with discrete phase (spray). Note that these two terms are distinct. The  $c_{\epsilon i}$  terms are model constants that account for compression and expansion. In the previous equation,  $R = 0$  for the standard  $k$ - $\epsilon$  model and

$$R = \frac{C_\mu \eta^3 \left(1 - \frac{\eta}{\eta_o}\right) \epsilon^2}{(1 + \beta \eta^3) k} \quad (1.29)$$

For the RNG  $k$ - $\epsilon$  model. In Equation 1.23

$$\eta = \frac{k}{\epsilon} |S_{ij}| = \frac{k}{\epsilon} \sqrt{2 S_{ij} S_{ji}} \quad (1.30)$$

The Rapid Distorsion RNG  $k$ - $\epsilon$  model uses the transport equation for  $\epsilon$  given by

$$\frac{\partial \rho \epsilon}{\partial t} + \frac{\partial \rho u_i \epsilon}{\partial x_i} = \frac{\partial}{\partial x_i} \left( \frac{\mu}{Pr_k} \frac{\partial \epsilon}{\partial x_j} \right) - \left[ \frac{2}{3} c_{\epsilon 1} - c_{\epsilon 3} + \frac{2}{3} c_\mu c_\eta \frac{k}{\epsilon} \frac{\partial u_k}{\partial x_k} \right] \rho \epsilon \frac{u_i}{x_i} + \left( c_{\epsilon 1} - c_\eta \frac{\partial u_i}{\partial x_j} \tau_{ij}^* - c_{\epsilon 2} \rho \epsilon + c_s S_s \right) \frac{\epsilon}{k} \quad (1.31)$$

where

$$c_\eta = \frac{\eta \left(1 - \frac{\eta}{\eta_o}\right)}{(1 + \beta \eta^3)} \quad (1.32)$$

And

$$\tau_{ij}^* = \tau_{ij} - \frac{1}{3} \delta_{ij} \tau_{kk} = 2\mu_\tau \left( S_{ij} - \frac{1}{3} \delta_{ij} \frac{\partial u_k}{\partial x_k} \right) \quad (1.33)$$

The source term,  $S_s$ , in Equations (1.27), (1.28), (1.31) is included to account for the interactions of turbulence with the discrete phase. This term is modelled as

$$S_s = - \frac{\sum_p N_p (F'_{drag,i} u'_i)_p}{V} \quad (1.34)$$

where the summation is over all parcels in the cell,  $N_p$  is the number of drops in a parcel,  $V$  is the cell volume,  $u'_i$  is the fluctuating component of the gas-phase velocity, and

$$F'_{drag,i} = \frac{F_{drag,i}}{u_i + u'_i - v_i} \quad (1.35)$$

where  $F_{drag,i}$  is the drag force on a drop. It is important to note that although the  $c_s$  model constant only appears in front of  $S_s$  in the transport equation, setting  $c_s$  to zero in the input files actually deactivate the source term in both

the  $k$  and  $\epsilon$  equations.

## 1.4 Mesh Generation

In every CFD calculation a proper choice of the grid is crucial. This choice strongly affect both the accuracy and the reliability of the results but also the time required to complete a simulation. The more the grid is fine the more the accuracy and the resolution of the results increase; but this leads obviously also to an increasing in the number of cells and so the time (strictly linked to the cost) of a simulation. Usually the best solution is a trade-off between the two issues.

These circumstances lead to the need of an appropriate knowledge of the system under observation for a proper optimization of the mesh; the critical point of the geometry must be found in order to set a refinement of the mesh only in that region. These points could be regions where neck are present, deviation of the flow, or where some particular phenomenon of the system happens, such as injection or ignition in an internal combustion engine. So a finer grid could be applied in these particular regions to get accurate results, while for computational time saving a coarse grid could be applied in the rest of the geometry.

The grid could also be adjusted with a finer or a coarser one according to the evolution in time of the simulation. If the simulation is not steady state a finer mesh may be used when the rate of variation of thermo-physical quantity is higher while a coarser one is to be preferred during non-critical simulation times. Proper algorithms are implemented in the CFD software to take in account this problem.

### 1.4.1 Grid Scaling

Grid scaling can greatly reduce runtime by coarsening the grid during non-critical simulation times, and grid scaling can help capture critical flow phenomena by refining the grid at critical simulation times. For example, consider an in-cylinder diesel engine simulation that includes spray and combustion modelling. During the spray and combustion, you will need a higher resolution to ensure accuracy. But during compression, lower resolution may be sufficient. Thus you can coarsen the grid during compression to reduce runtime and refine the grid when the spray begins. [10]

### 1.4.2 Fixed Embedding

Use fixed embedding to refine the grid only in specific locations in the domain where a finer resolution is critical to the accuracy and precision of the solution. For example, when simulating sprays, you can add an area of fixed embedding by the nozzle to resolve the complex flow behaviour. Fixed embedding allows the rest of the grid to remain coarse to minimize simulation time [10].

### 1.4.3 Adaptive Mesh refinement

Use Adaptive Mesh Refinement (AMR) to automatically refine the grid based on fluctuating and moving conditions such as temperature or velocity. This option is useful for using a highly refined grid to accurately simulate complex phenomena such as flame propagation or high velocity flow without unnecessarily slowing the simulation with a globally refined grid. Ideally, a good AMR algorithm will add higher grid resolution (embedding) where the flow field is most under-resolved or where the sub-grid field is the largest (i.e., where the curvature [gradient] of a specified field variable is the highest) [10].

For a scalar, the sub-grid field is defined as the difference between the actual field and the resolved field

$$\phi' = \phi - \bar{\phi} \quad (1.36)$$

where  $\phi$  is the actual scalar field,  $\bar{\phi}$  is the resolved scalar field, and  $\phi'$  is the sub-grid scalar field. The sub-grid for any scalar can be expressed as an infinite series and is given by

$$\phi' = -\alpha_{[k]} \frac{\partial^2 \bar{\phi}}{\partial x_k \partial x_k} + \frac{1}{2} \alpha_{[k]} \alpha_{[l]} \frac{\partial^4 \phi}{\partial x_k \partial x_k \partial x_l \partial x_l} - \frac{1}{3} \alpha_{[k]} \alpha_{[l]} \alpha_{[m]} \frac{\partial^6 \phi}{\partial x_k \partial x_k \partial x_l \partial x_l \partial x_m \partial x_m} + \dots \quad (1.37)$$

where  $\alpha_{[k]}$  is  $dx_{k^2}$  for a rectangular cell and the brackets, [ ], indicate no summation. Since it is not possible to evaluate the entire series, only the first term (the second-order term) in the series is used to approximate the scale of the sub-grid or

$$\phi' \approx -\alpha_{[k]} \frac{\partial^2 \bar{\phi}}{\partial x_k \partial x_k} \quad (1.38)$$

Note that the above equations can be easily generalized for a vector field, such as velocity. A cell is embedded if the absolute value of the sub-grid field is above a user-specified value. Conversely, a cell is released (i.e., the embedding is removed) if the absolute value of the sub grid is below 1/5th of the user-specified value [10].

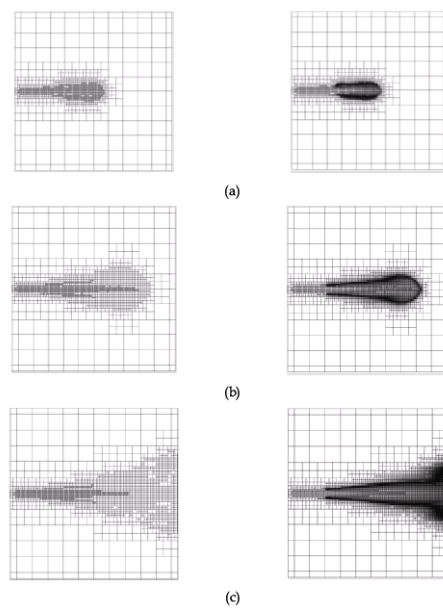


**Figure 1.7:** Evolution of a combustor spray bomb. This grid was generated by AMR (a) 0.5, (b) 1.0, and (c) 2.0 milliseconds after the start of the simulation. The left column shows the grid only, while the right column shows the grid and temperature values (black represents a temperature of approximately 2800K) for corresponding times. This case has an ambient temperature of 1000 K, an ambient density of  $14.8 \text{ kg/m}^3$ , an orifice diameter of 0.180mm, and an injection pressure of 136 Mpa



## Chapter 2

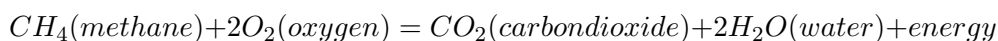
# Natural Gas — Why is Methane a Clean Fuel?

### 2.1 Introduction To Methane

What we call natural gas is mostly the chemical compound methane (95% or more; the rest is ethane or longer carbon chains). Methane, which comes out of the ground as a gas, is produced when microorganisms known as methanogens feed on organic matter in environments with little or no oxygen. It is abundant, seeping out of your garbage, landfills, and swamps. Also, everywhere you find oil, you find methane, usually in a pocket above the oil deposit. This methane emanated from the same organic material (dead plants and animals) that produced the oil. Methane can be captured where it naturally occurs or produced in a controlled environment like an anaerobic digester. After it is captured or produced, it is cleaned (by removing carbon dioxide and other liquids); compressed to a higher pressure; odorized (it's odorless and lethal in high doses in its natural state); and piped into our homes, power plants, and factories for heat and power.

### 2.2 Clean Combustion

Methane, like all fossil fuels, can be combusted (reacted with oxygen) to form energy and water. In fact, a large and growing part of our electricity supply comes from methane. It is the simplest fossil fuel — a single carbon atom with four hydrogen atoms, or CH<sub>4</sub>. Compare that to diesel fuel, which is a soup of long-chained carbons with sulfur and other molecules attached. The basic methane combustion reaction is[11]:



Because of its simplicity and lack of additional compounds, methane is the cleanest of the fossil fuels to combust. When we say cleanest, though, we often mean different things. In terms of the production of carbon dioxide (i.e., the major greenhouse gas), methane has the lowest density, meaning we get more energy per unit of carbon dioxide than we do with other fuels. It releases 29% less carbon than oil, 43% less than coal, and 20-30% less lifecycle carbon than oil when used as a transportation fuel. In addition, unlike other fuels,

methane combustion results in basically no NO<sub>x</sub> (nitrous oxide), SO<sub>x</sub> (sulfur dioxide), or particulate matter being released into the atmosphere. These gases are all dangerous to our health and regulated under the Clean Air Act. Fossil fuels and their energy density[11]:

natural gas (51.6 kJ/g) > petroleum (43.6 kJ/g) > coal (39.3 kJ/g) > ethanol (27.3 kJ/g) > wood (16.1 kJ/g)

It should be noted that methane, by itself, when released into the atmosphere, is a potent greenhouse gas. It captures heat [70 times] better and thus, by weight, is 70 times as dangerous as carbon dioxide. This is why it's so important to flare methane to ensure that it is completely combusted into carbon dioxide. It also means that it is critical that the infrastructure to transport methane — drilling sites, pipes, and tanks — minimizes any leakage into the air. Otherwise, the benefit of transitioning from coal to natural gas (in terms of greenhouse gases) would quickly be lost.

### 2.3 The Age of Methane

The increased use of methane in the US, predominately replacing coal, has stabilized if not actually lowered our level of emissions, and the retirement of old coal power plants is eliminating one of the country's largest polluters. Energy transitions typically move from a lower density fuel to a higher density fuel. We moved from wood to coal to oil, and now methane is creeping up, passing coal to become the second largest source of energy in the US. While denser, it is also a gas, which presents logistical issues for transport and storage. Nonetheless, I think we will eventually make the transition from oil to methane, at least in the US, before renewables ultimately take over in the second half of this century. And when they do, it will be because technically they are a better fuel — i.e., more energy dense.

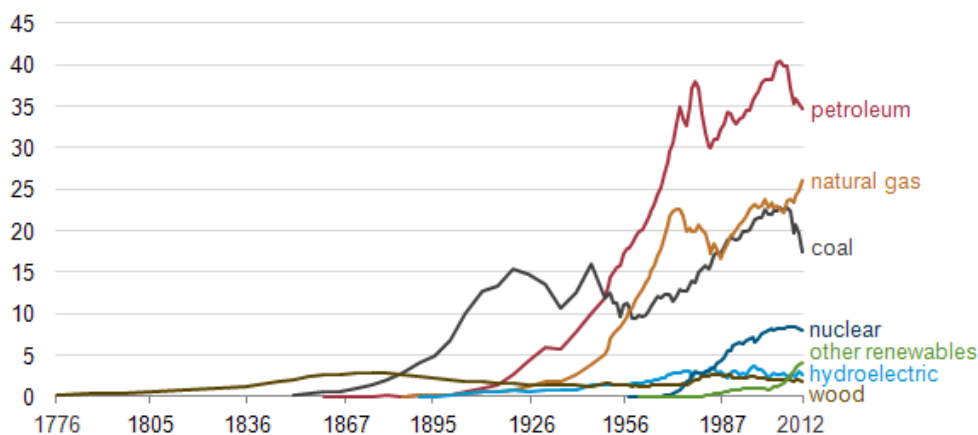


**Figure 2.1:** History of energy consumption in US (1776-2012)[11]

## 2.4 Global Dynamics

As discussed, methane, being a gas, presents a transportation challenge. The US has a vast network of pipelines, and Russia pipes compressed natural gas into Europe and China from their vast reserves. However, in order to physically move natural gas, as opposed to transferring it via pipeline, you need to cool it to a liquid (at -260 degrees Fahrenheit), at which point it becomes liquified natural gas, or LNG (in it's compressed form, it's called compressed natural gas, or not surprisingly, CNG). Once liquified, it can then be transported via ship.

Less than 10 years ago, the US built import terminals to import LNG from abroad. More recently, however, with the discovery of new drilling techniques (i.e., fracking), those same terminals have been re-configured as export terminals as the US is now one of the world's leading producers of natural gas, along with Russia and Qatar. However, the difficulty and, thus, cost to move it has created a huge pricing disparity around the world. For example, natural gas is routinely under \$5/MMBTU in the US, while it can be as much as \$20/MMBTU in Japan or China. This has put a huge amount of pressure on producers to export to Asia to satisfy growing demand, as well as on the Asian countries to produce more gas themselves through a combination of the gasification of coal and importing drilling technologies from the US. Just 10 years ago, the US was scared of running out of fuel, but now we find ourselves with an abundance; Asia, by importing fracking technology, could very well find itself in a similar situation.

---



## Chapter 3

# The Effect of Air-Fuel Ratio ( $\lambda$ ) on Combustion

### 3.1 Stoichiometric Combustion Reaction

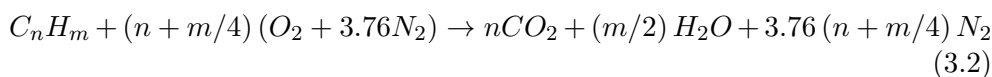
A Complete combustion is a consequence of the reaction of a fuel with oxygen as an oxidizer, to produce carbon dioxide ( $CO_2$ ) and water ( $H_2O$ ). The combustion process is always exothermic which releases energy from the system to its surroundings. The combustion reaction may be written as[8]:



Since fuels are burned in the air rather than in pure oxygen, the nitrogen in the air may participate in the combustion process to produce nitrogen oxides. Also, many fuels contain elements other than carbon, and these elements may be transformed during combustion. Finally, combustion is not always complete, and the flue gases contain unburned and partially burned products in addition to  $CO_2$  and  $H_2O$ .

Air is formed by oxygen, nitrogen, and small amounts of carbon dioxide, argon, and other gases. Since the majority of the air is occupied by nitrogen, for our purposes it is quite a reasonable approximation to consider air as a mixture of 21% oxygen and 79% nitrogen. Hence, for every mole of oxygen required for combustion, 3.76 mol of nitrogen must be introduced.

The stoichiometric relation for complete oxidation of a hydrocarbon fuel turns out to be[8]:



### 3.2 Air-Fuel Ratio

Internal combustion Engines require a mixture of fuel and oxygen (from air) to produce energy through combustion. Therefore, certain amounts of fuel and air (depending on the type of the fuel) required in order to have an efficient combustion behavior. A complete combustion (3.1),(3.2) takes place when all the fuel is burned, while in flue gas there won't be any quantities of unburned fuel. Air-fuel ratio (AF or AFR) is the ratio between the mass of air  $m_a$  and

mass fuel  $m_f$  which can be represented by[12]:

$$ATF = \frac{m_a}{m_f} \quad (3.3)$$

### 3.2.1 Stoichiometric Air-Fuel Ratio

Stoichiometric air-fuel ratio indicates the ratio related to the exact amount of air presented in the engine to burn the fuel completely.

This ratio is used to determine the perfect ratio of air and fuel which leads to achieving an efficient performance of the engine.

When the air-fuel ratio is higher than the stoichiometric ratio, the air-fuel mixture is called lean. When the air-fuel ratio is lower than the stoichiometric ratio, the air-fuel mixture is called rich.

The table below, reports the stoichiometric air-fuel ratio for some fossil fuels. According to the Table 3.1, as an example, in order to burn completely 1 kg

Fuel	Chemical Formula	AFR
Methane	$CH_4$	17.19:1
Diesel	$C_{12}H_{23}$	14.5:1
Hydrogen	$H_2$	34.3:1
Gasoline	$C_8H_{18}$	14.7:1
Methanol	$CH_3OH$	6.47:1

**Table 3.1:** the stoichiometric air-fuel ratio for some fossil fuels[12]

of Methane, we need 17.19 kg of air while for Hydrogen this amount reaches to 34.3 kg, which refers to the stoichiometric air-fuel ratio.

### 3.2.2 Air-fuel ratio equivalence factor – $\lambda$

In reality, internal combustion engines do not work exactly with ideal AFR, but with values close to it. Therefore we'll have an ideal and a actual air-fuel AFR. The ratio between the actual air-fuel ratio ( $AFR_{actual}$ ) and the ideal/stoichiometric air-fuel ratio ( $AFR_{stoich}$ ) is called equivalence air-fuel ratio or lambda ( $\lambda$ )[12].

$$\lambda = \frac{AFR_{actual}}{AFR_{stoich}} \quad (3.4)$$

also,

$$\phi = \frac{1}{\lambda} \quad (3.5)$$

Depending on the value of lambda, the engine is told to work with lean, stoichiometric or rich air-fuel mixture.

Equivalence factor	Air-Fuel mixture type	Description
$\lambda < 1.0$	Rich	There is not enough air to burn completely the amount of fuel; after combustion, there is unburnt fuel in the exhaust gases
$\lambda = 1.0$	Stoichiometric (ideal)	The mass of air is exact for a complete combustion of the fuel; after combustion, there is no excess oxygen in the exhaust and no unburnt fuel
$\lambda > 1.0$	Lean	There is more oxygen than required to burn completely the amount of fuel; after combustion, there is excess oxygen in the exhaust gases

**Table 3.2:** Types of combustible mixtures[12]

### 3.3 How does the air-fuel ratio affect the engine performance?

Air-fuel ratio plays a decisive role in the performance of the engine. More specifically, affects the power generation and the amount of fuel consumption. Figure 3.1 displays the dependency of mentioned terms to the AFR. it shows, by having a lean mixture ( $\lambda > 1.0$ ) the lowest fuel consumption is achievable and the main reason behind is the availability of sufficient oxygen to burn the whole fuel completely which turns into mechanical work, While in terms of generating the maximum power, the mixture ratio acts conversely and varies from lean to rich ( $\lambda < 1.0$ )[12].

Actually, the excess of fuel in the cylinder cools down the combustion chamber (through fuel evaporation and heat absorption) which finally leads to produce the maximum power.

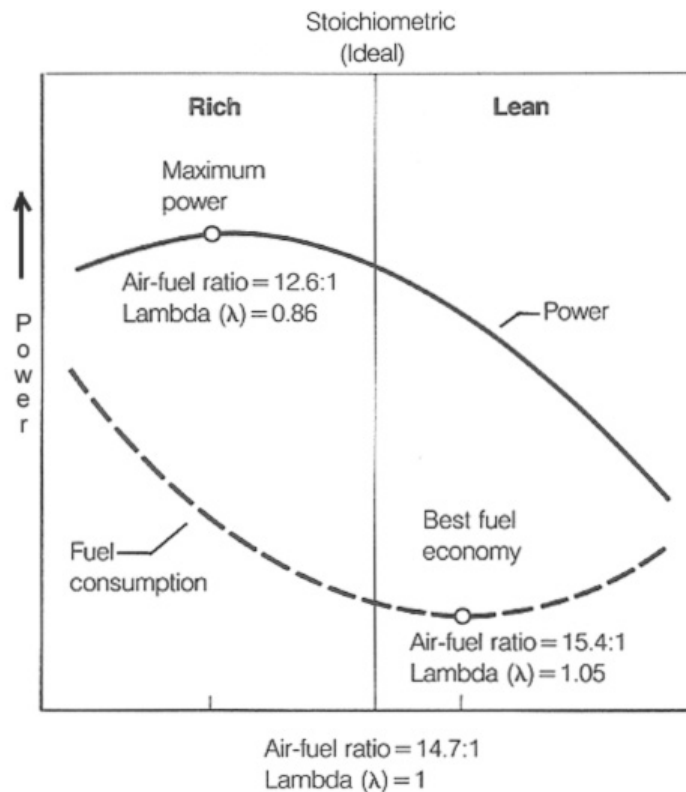


**Figure 3.1:** Engine power and fuel consumption as a function of air-fuel ratio ( $\lambda$ ) for Gasoline[9]

The best assumption would be of having the maximum power of the engine with the lowest fuel consumption with the same air-fuel ratio, but the figure determines this assumption is not feasible.

The figure 3.1 shows in detail for gasoline, the lowest fuel consumption (best fuel economy) is achieved with lean mixtures, with an AFR of 15.4:1 and  $\lambda$  of 1.05. The maximum engine power is produced with rich mixtures, with an AFR of 12.6:1 and  $\lambda$  of 0.86.

In fact, there is a sort of trade-off between maximum engine power and minimum fuel consumption.

## Chapter 4

# Turbulent Length Scales

This report compares the cycle to cycle behavior of turbulent flows for Gason and Polito engines and investigates the corresponding mesh resolutions. To do so we are going to deal with a wide range of turbulent length scales (eddy sizes) or even more specifically, studying the Kolmogorov and integral turbulent length scales which are planned to have a brief explanation through the latter part of the report.

### 4.1 introduction

Turbulent flow at high Reynolds number  $Re = \frac{UL}{\nu}$  is composed of eddies of varying sizes which can be observed in the Figure 4.1. The size defines a

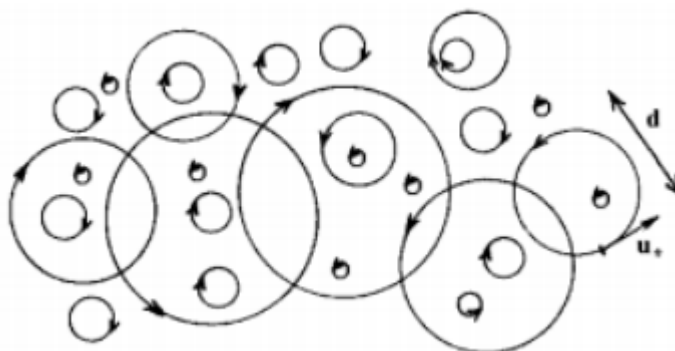


**Figure 4.1:** Turbulent flow composed of multi-sized eddies[17]

characteristic length scale for the eddies which are also characterized by flow velocity scales and timescales (turnover time). The size of the largest eddies in flow will be given by  $L_t$  so-called **integral length scale** and the smallest eddies by  $\eta$  which refers to **Kolmogorov length scale**.

### 4.2 Kolmogorov length scale

Kolmogorov's first hypothesis states, the only factors influencing the behavior of the small scales motions are the overall kinetic energy production rate and viscosity. The dissipation rate will be independence of viscosity, but the scales at which this energy is dissipated will depend on both the dissipation rate

and viscosity. The dissipation rate per unit mass  $\varepsilon = \frac{u^3}{l_0}$  has dimension  $(\frac{m^2}{s^3})$  and viscosity ( $\nu$ ) has dimension  $(\frac{m^2}{s})$ , then the length scale formed from these quantities is:

$$\eta = \left(\frac{\nu^3}{\varepsilon}\right)^{1/4} \quad (4.1)$$

This quantity which is the smallest length scale is called Kolmogorov length scale. Actually, eddies smaller than Kolmogorov scale will be instantly dissipated by viscosity.

Note that the Kolmogorov Reynolds number  $Re_\eta$  of the small eddies is 1.

### 4.3 Internal Length Scale

For very high Reynolds number flows, the viscous forces become increasingly small with respect to the inertial forces. The length scales of those eddies can be defined as:

$$l_0 \propto \frac{k^{3/2}}{\varepsilon} \quad (4.2)$$

Where k refers to turbulent kinetic energy  $(\frac{m^2}{s^2})$ .

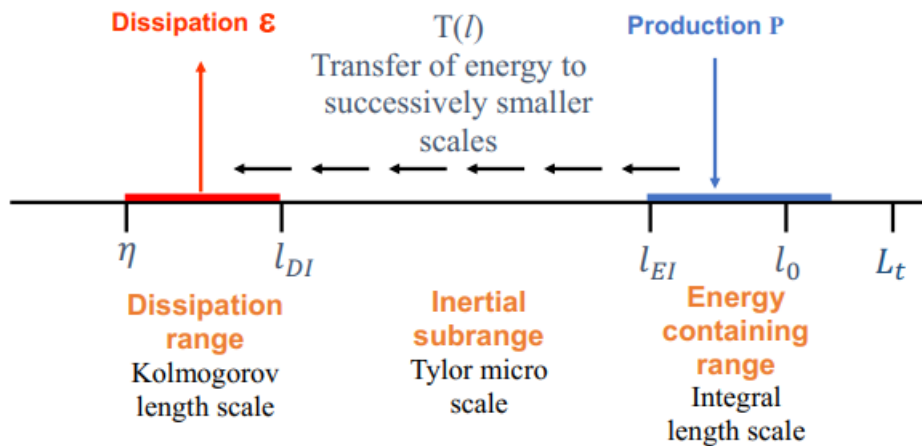


**Figure 4.2:** Different length scales and ranges in turbulence energy cascade[18]

### 4.4 Energy Transfer

The largest eddies which have been fed by external force are unstable and eventually break up, transferring their energy to somewhat smaller eddies. These smaller eddies undergo a similar break-up process and transfer their energy to yet smaller eddies. This process is known as the turbulent energy cascade – in which energy is transferred to successively smaller and smaller eddies – continues until the Reynolds number is sufficiently low where the fluid viscosity is dominant and effectively dissipate the kinetic energy into heat.

### 4.4.1 Energy Spectrum

The turbulent kinetic energy  $k$  is given by:  $k = \frac{1}{2} \langle u_i u_i \rangle = \frac{1}{2} (u'^2 + v'^2 + w'^2)$ . The distribution of turbulent kinetic energy between the eddies of varying sizes is determined by energy spectrum  $E(\kappa)$ .

Here  $E(\kappa)$  is the energy contained in eddies of size  $l$  and wavenumber  $\kappa$ , defined as:

$$k = \int_0^{\infty} E(\kappa) d(\kappa) \quad (4.3)$$

### 4.4.2 Full Spectrum

As has been shown on the Figure, it is composed of 3 regions where Energy containing range stands for large eddies where the viscous dissipation is not very important.

Within inertial range, eddies are much larger than dissipative eddies that

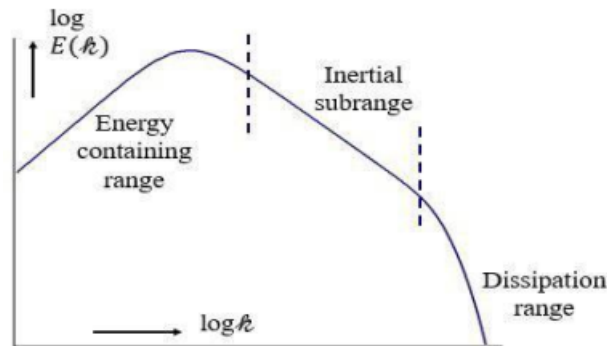


**Figure 4.3:** Energy spectrum of turbulent flow[18]

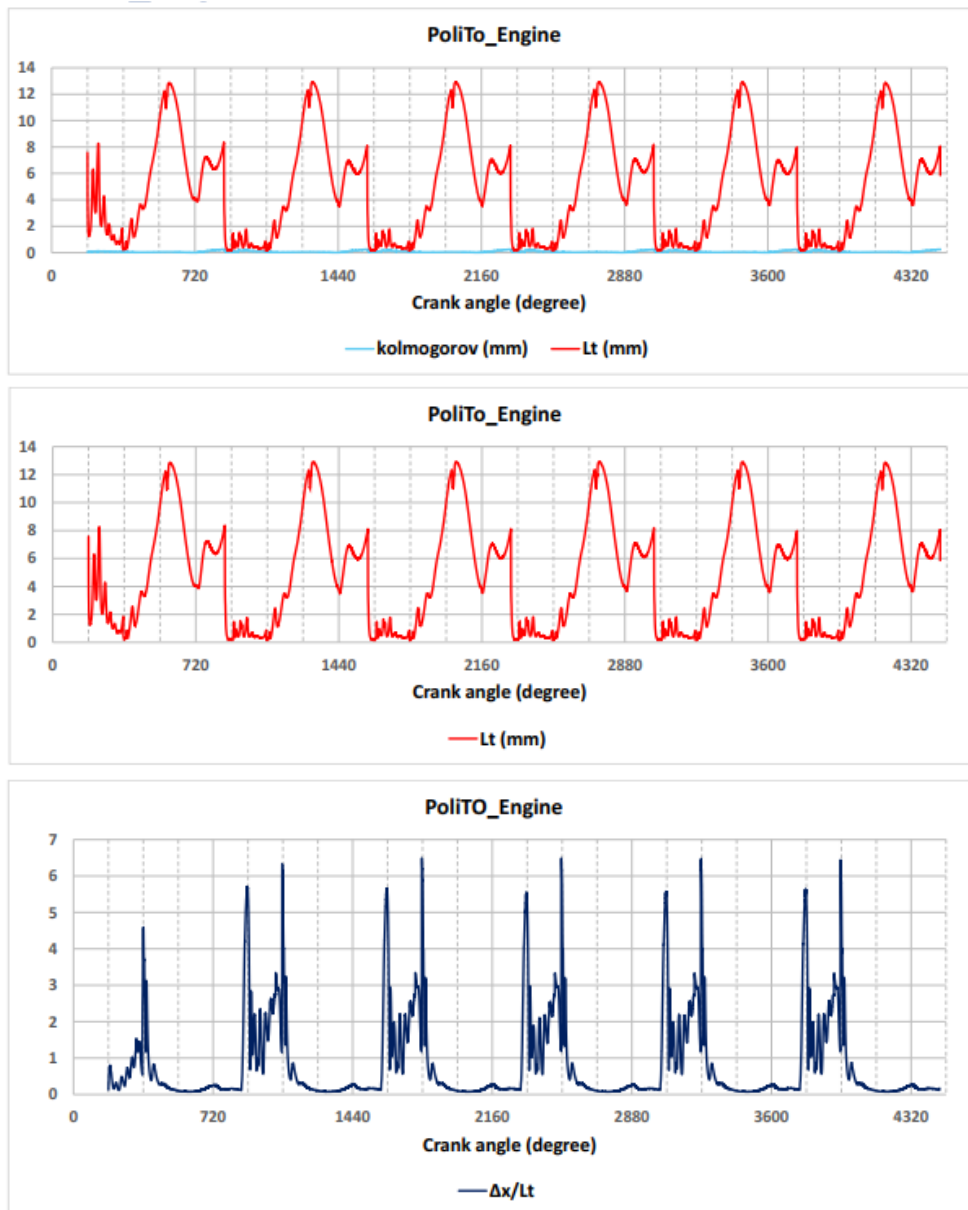
exists at Kolmogorov scales, energy is essentially not dissipated in this range. Within this range the inertial effect is still much larger than viscous efforts and can be assumed that viscosity doesn't play a role. Lastly, within dissipation range viscosity is dominant and we can say the energy is lost to viscous dissipation.

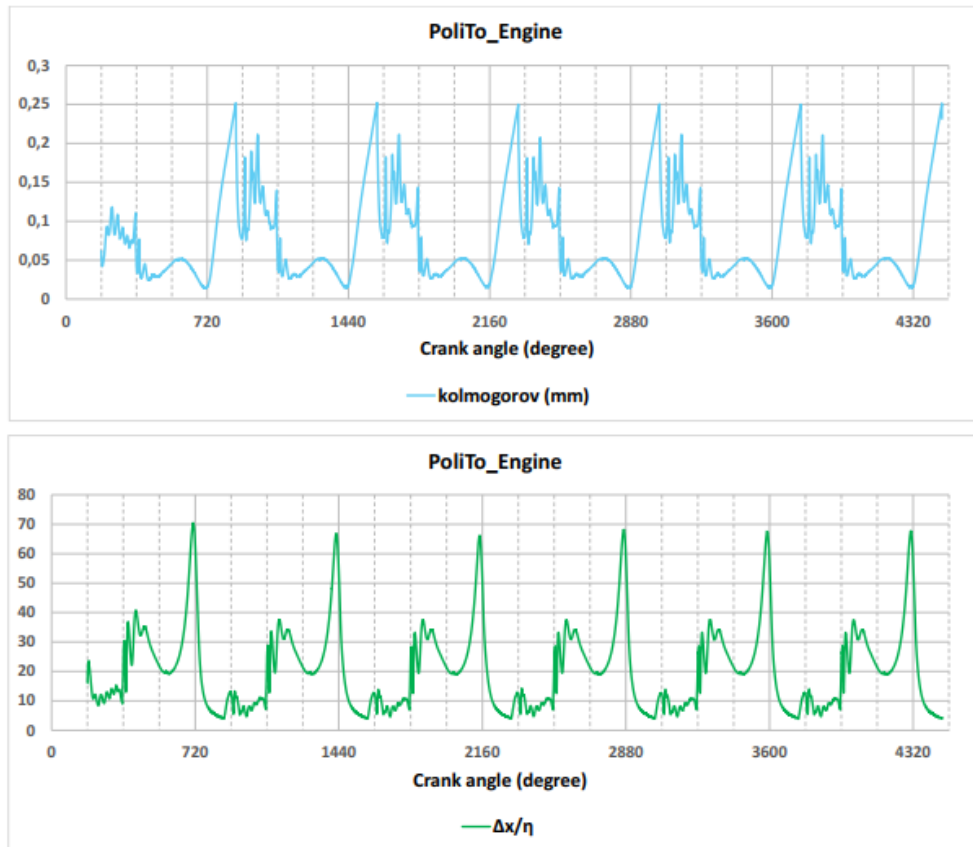
## 4.5 Procedure

During a multistage simulation of Polito engine, up to the 3rd cycle, we observed quietly high cycle to cycle variation, while afterwards, up to the sixth cycle we experienced very slight variation. We planned to investigate some quantities of the turbulent flow such as integral length scale, Kolmogorov length scale and making a ratio of cell size over Kolmogorov length scale and compare them with GasOn project which has been already done by the other colleagues.

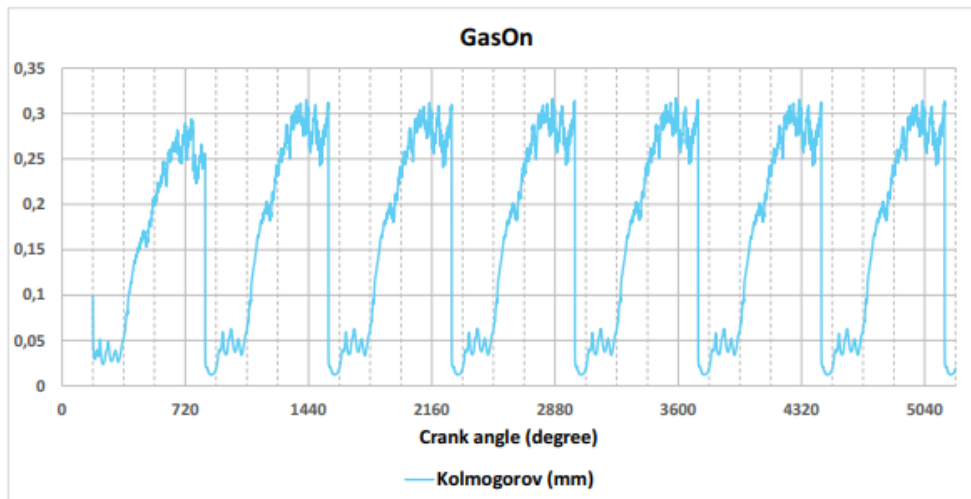
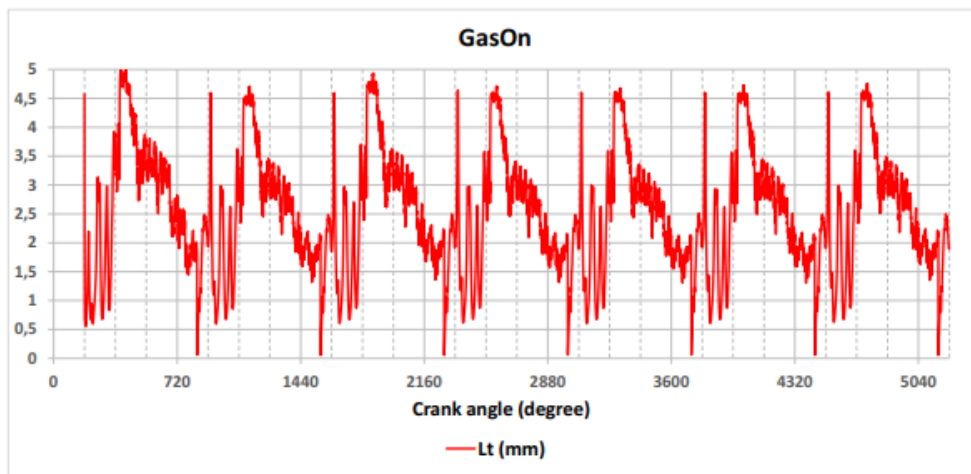
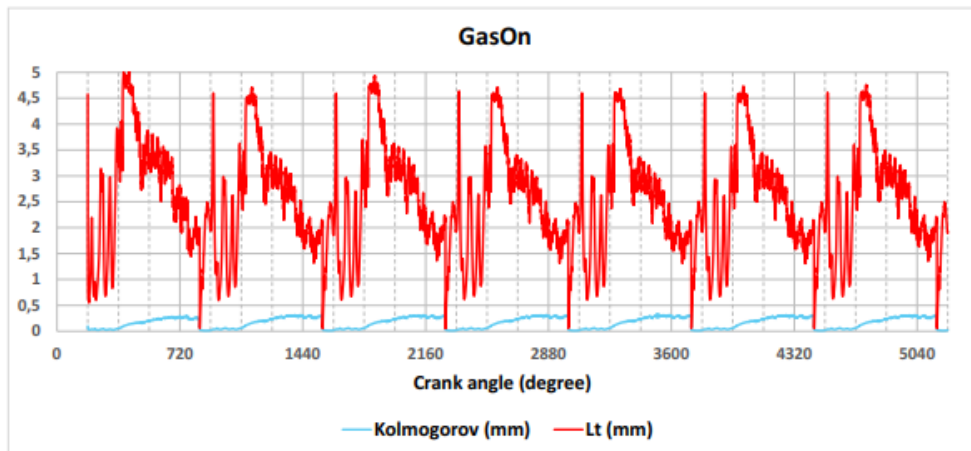
It is important to highlight that, at Polito engine we are dealing with the case 2000x6, finer mesh with  $\lambda=1$  and for GasOn project is 2000x8. where, for the finer mesh the cell size has been chosen  $\Delta x = 1$  mm with  $\lambda=1$ . We extracted the data from the software so as to create some plots which let us to have a clear distinction between the two processes.

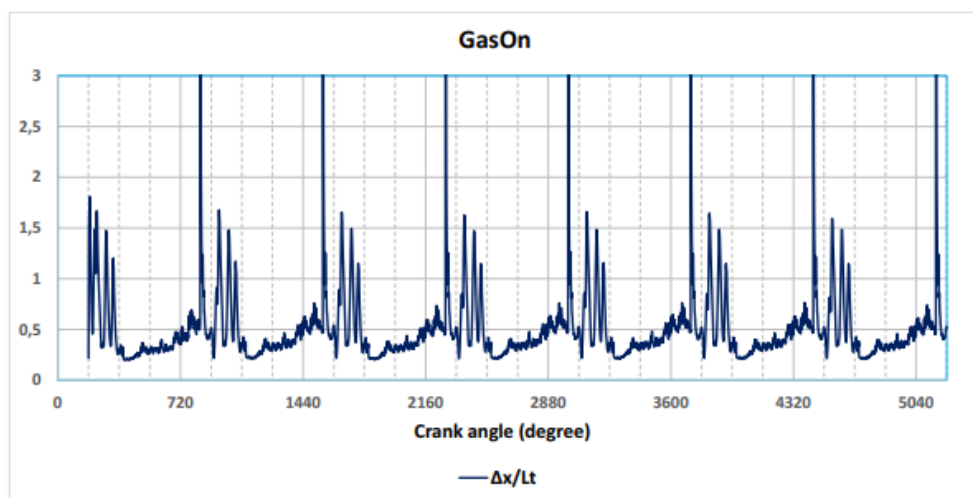
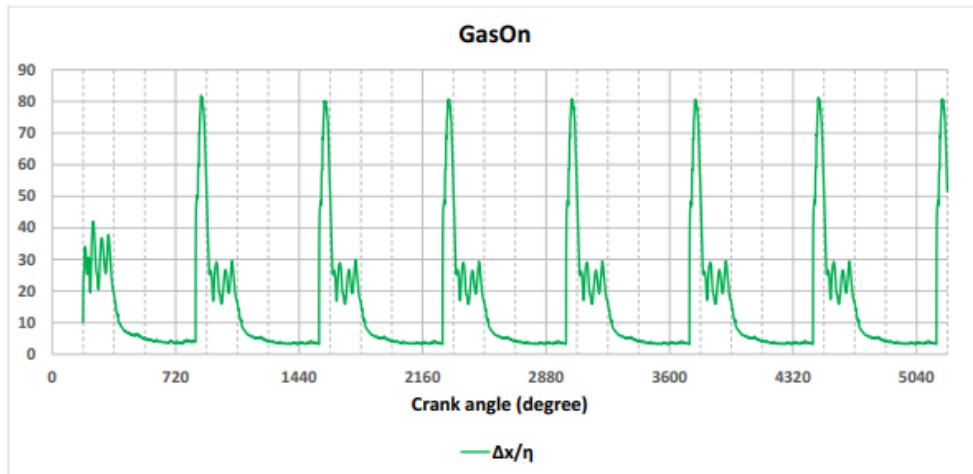
## 4.5.1 Polito Engine Figures



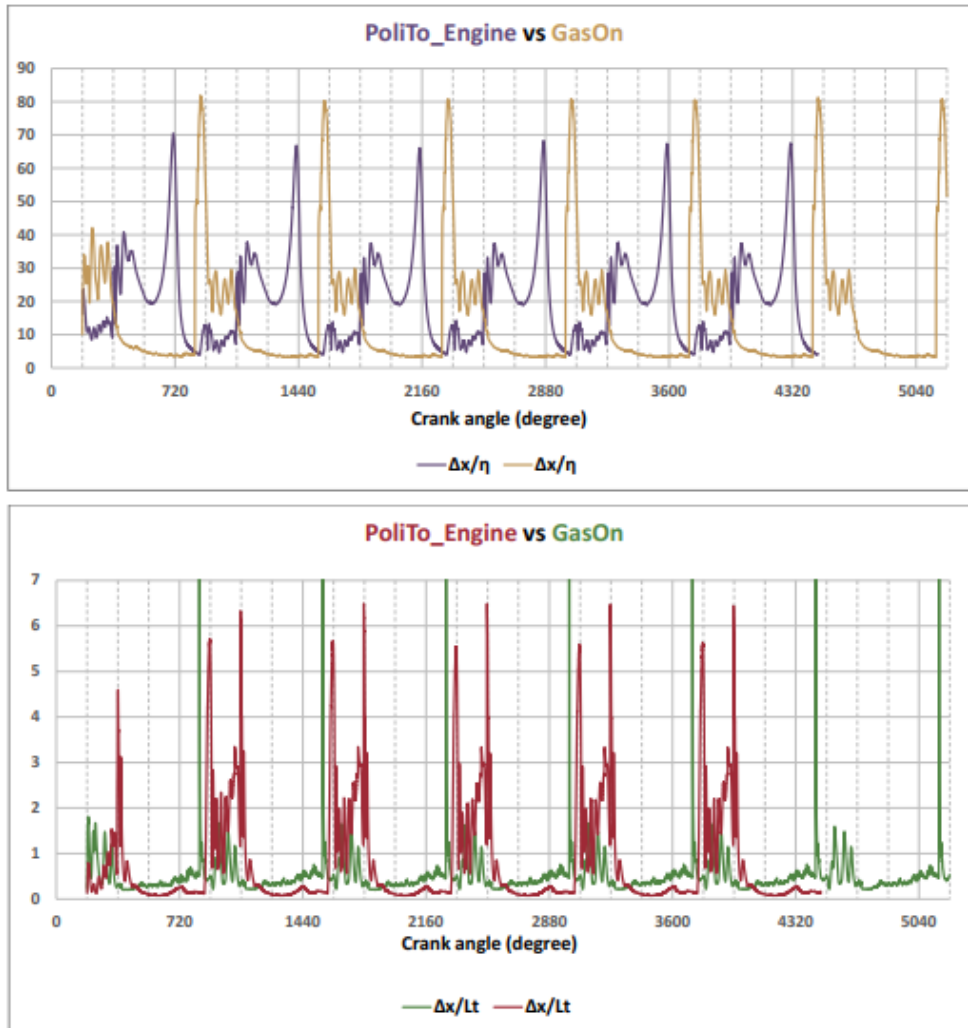


## 4.5.2 GasOn Figures





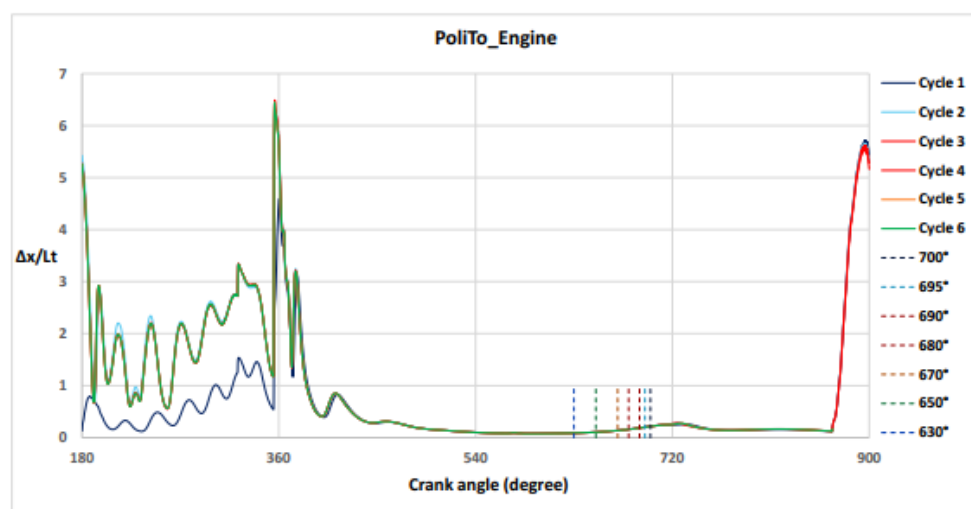
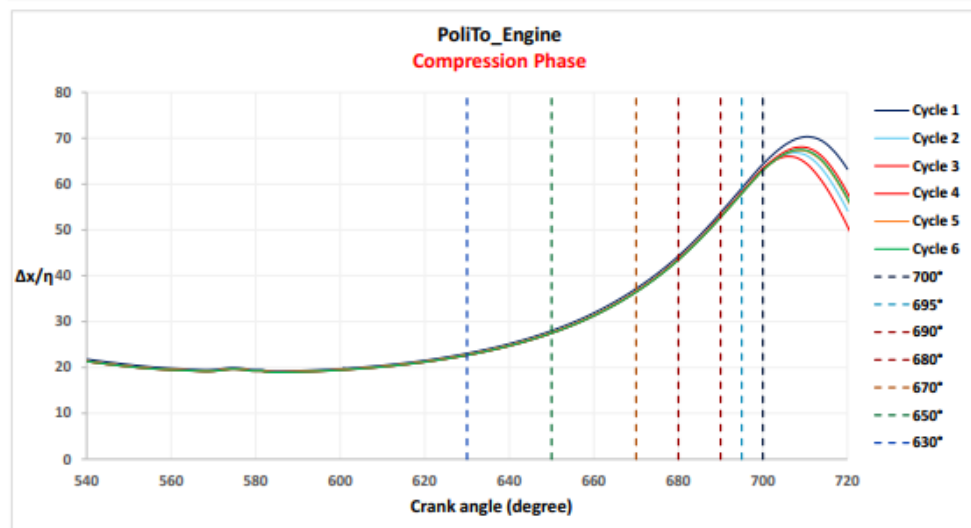
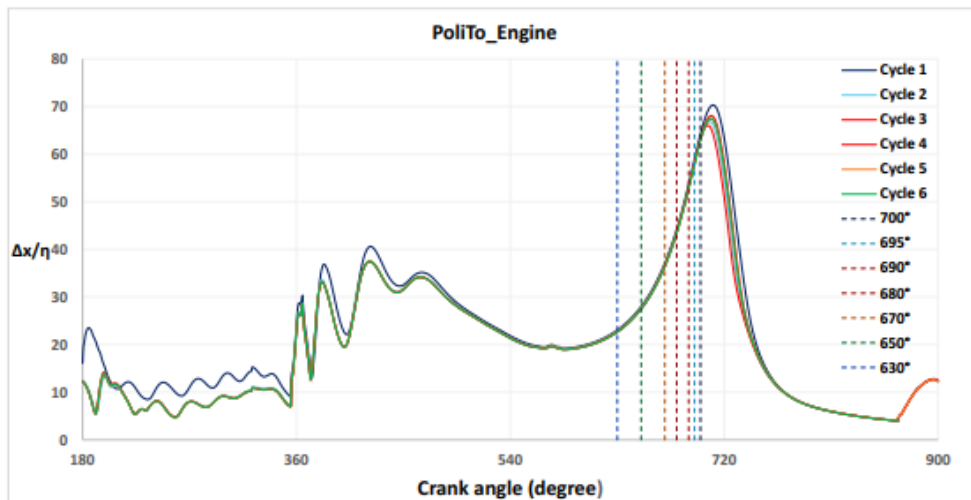
### 4.5.3 Polito Engine VS GasOn

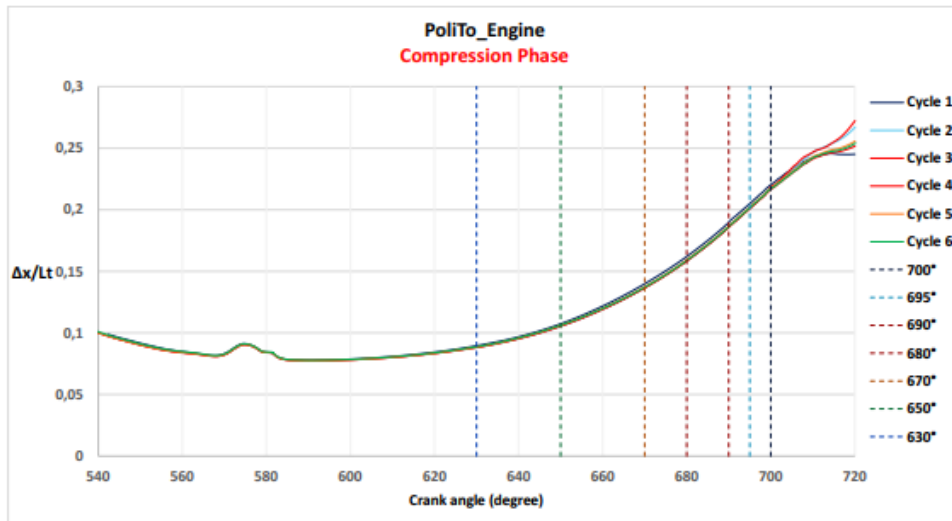


### 4.5.4 Ensembling

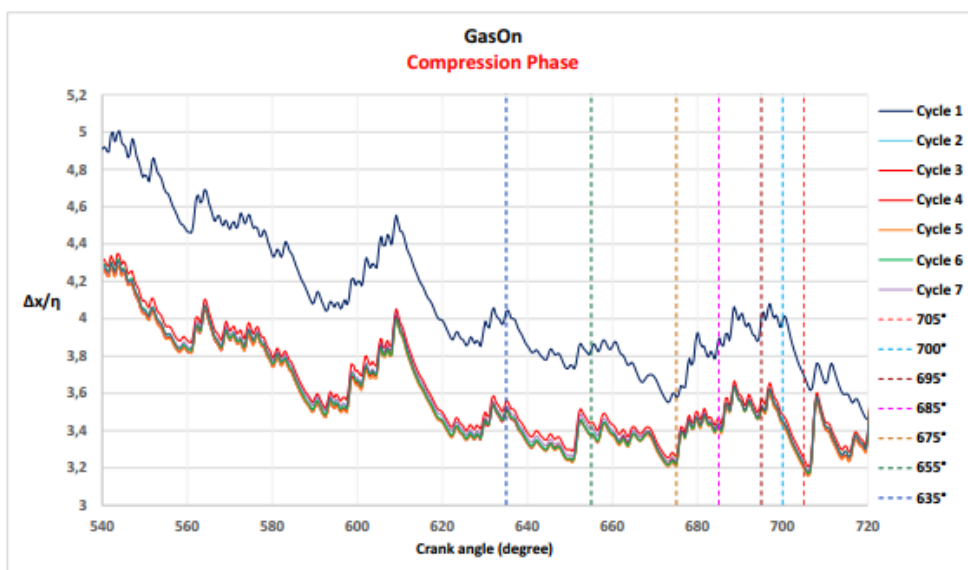
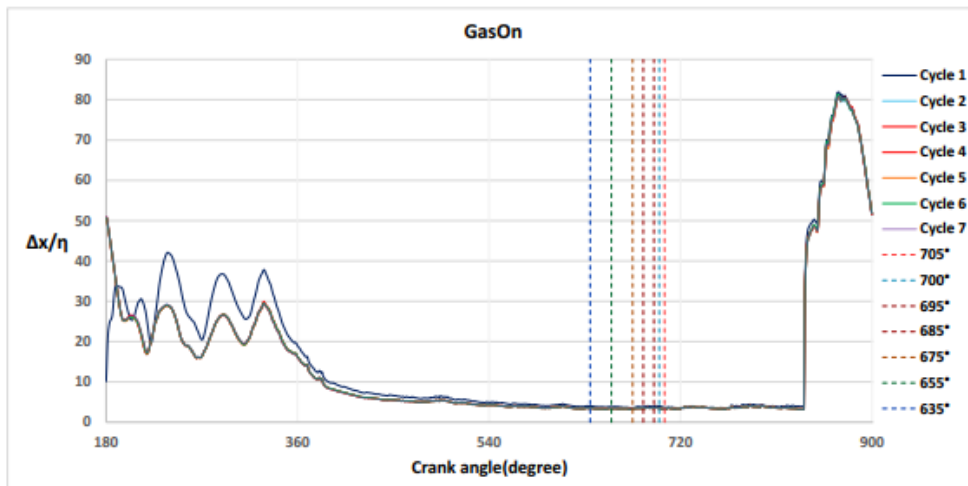
As is observed from the former figures, the cycles proceeded continuously, but what we ultimately want, is to distinguish how each cycle varies respect to each other, for this objective, to have a close-up view, we can superimpose the cycles on a plane and spotting the crank angles which are important to us. For GasOn engine  $SA = 704^\circ$ , actually  $16^\circ$  before TDC, hence the investigating angles are  $\theta = 705, 700, 695, 685, 675, 655$  and  $635$  degrees, while for Polito engine  $SA = 698^\circ$ , so the angles turn out to be  $\theta = 700, 695, 690, 680, 670, 650$  and  $630$  degrees

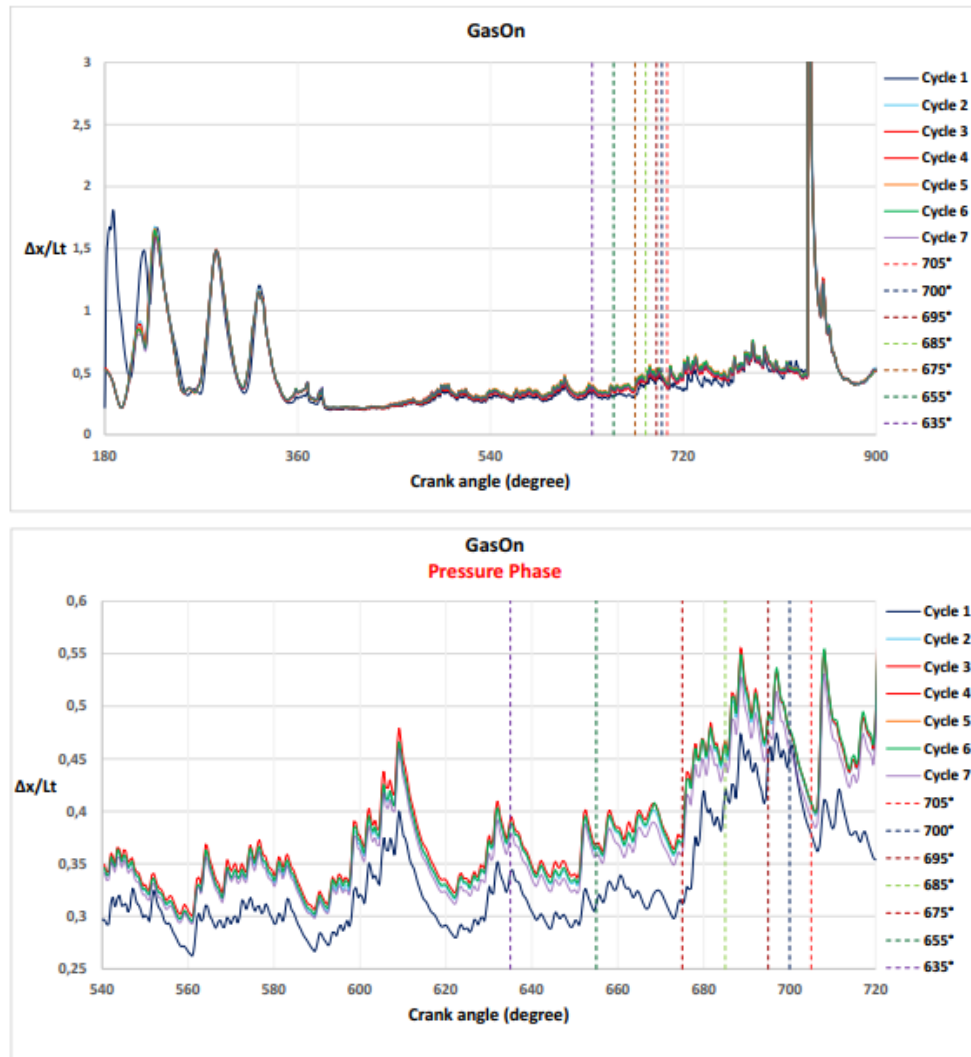
Polito Engine





## GasOn



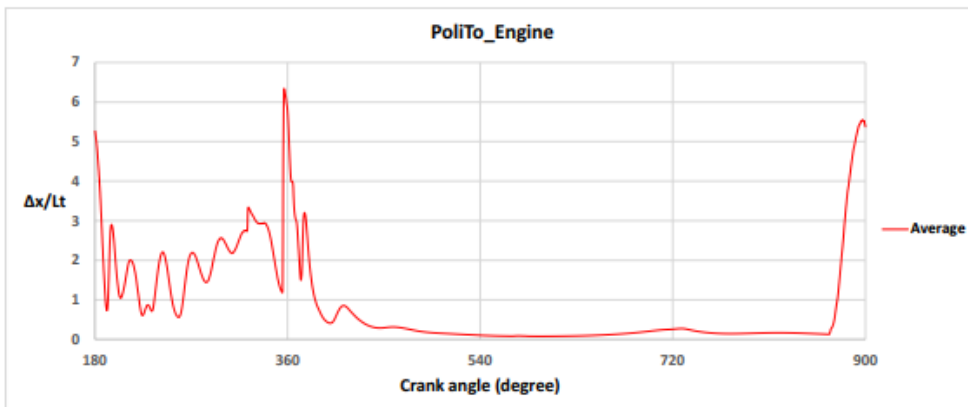
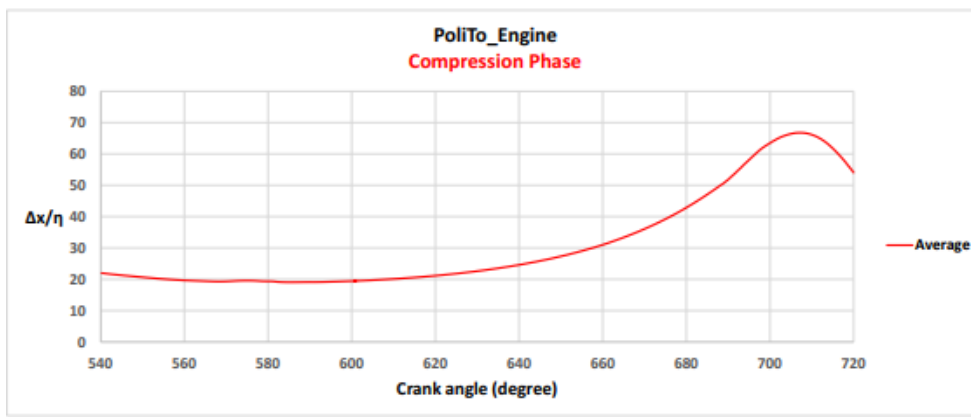
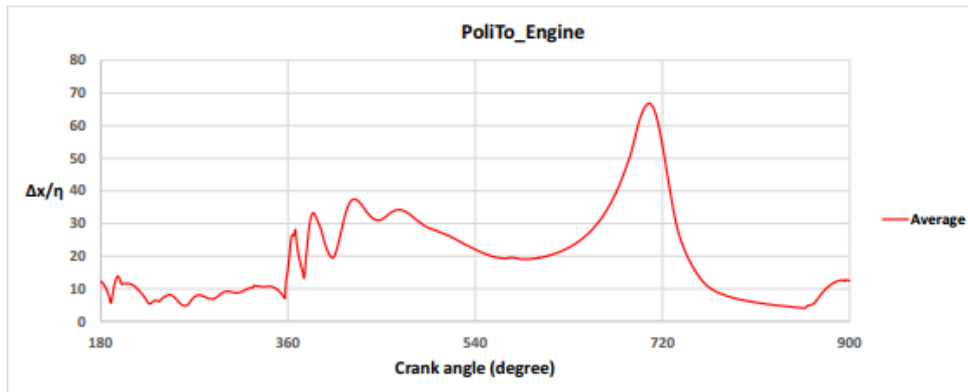


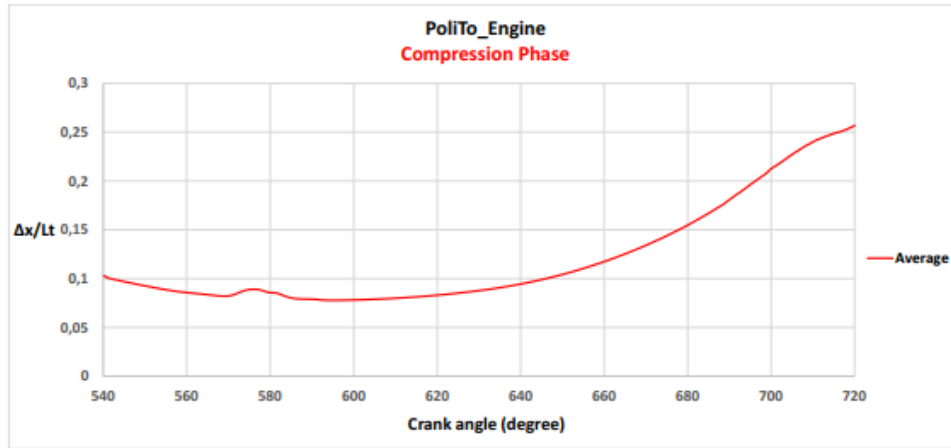
We see for both cases (Polito Engine GasOn) a notable feature which is the trend of the first cycle that proceeds differently than the others, while from the 2nd cycle up to the last one the cycles are more or less matching each other.

We can claim that the first cycle is not a correct cycle because for the model to start we apply some values for the boundary condition such as temperature and pressure, thus the first cycle will work under imposed boundary condition, but from the 2nd cycle onward, after the interaction of quantities, we get more realistic values.

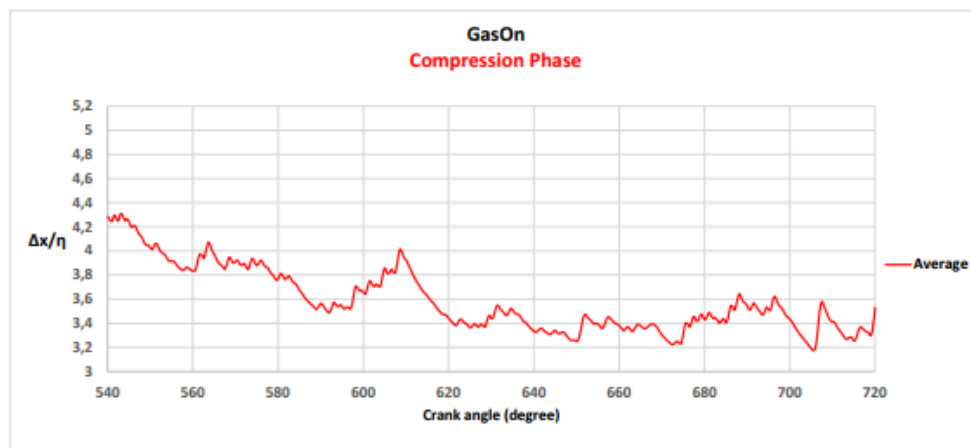
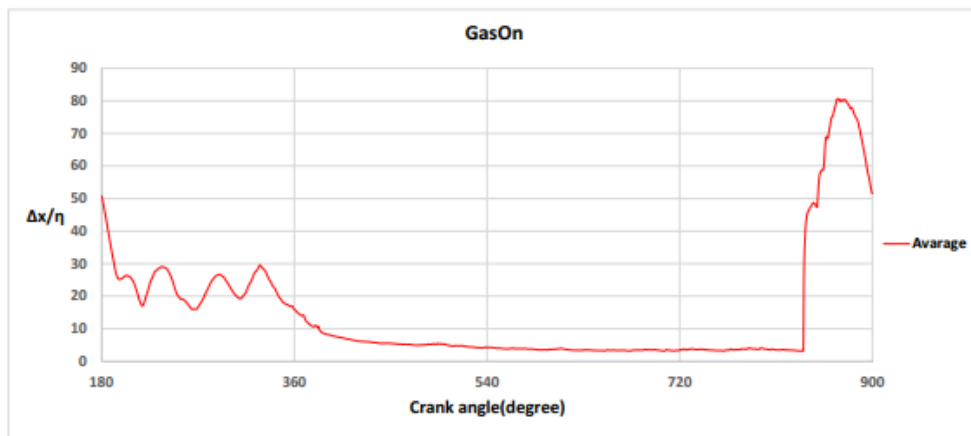
According to the explanation above, we cancel the first cycle, and take an average from the others.

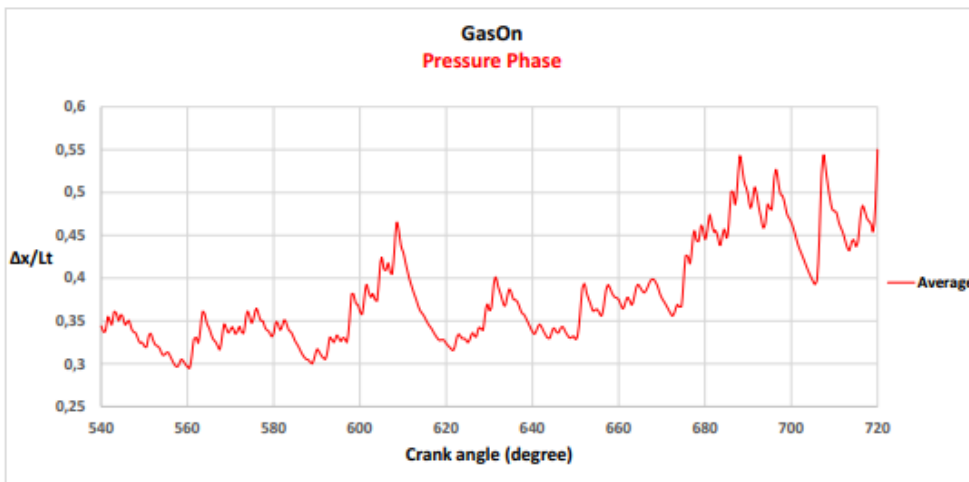
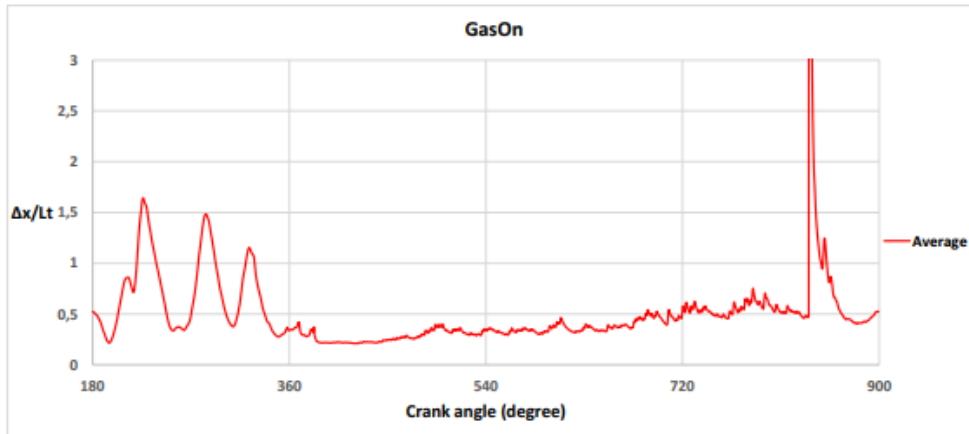
## Ensembling (Polito Engine)



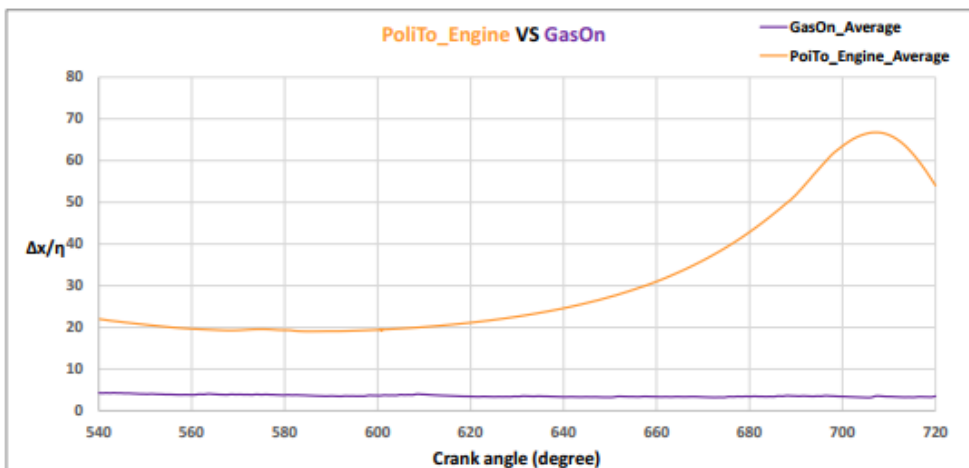


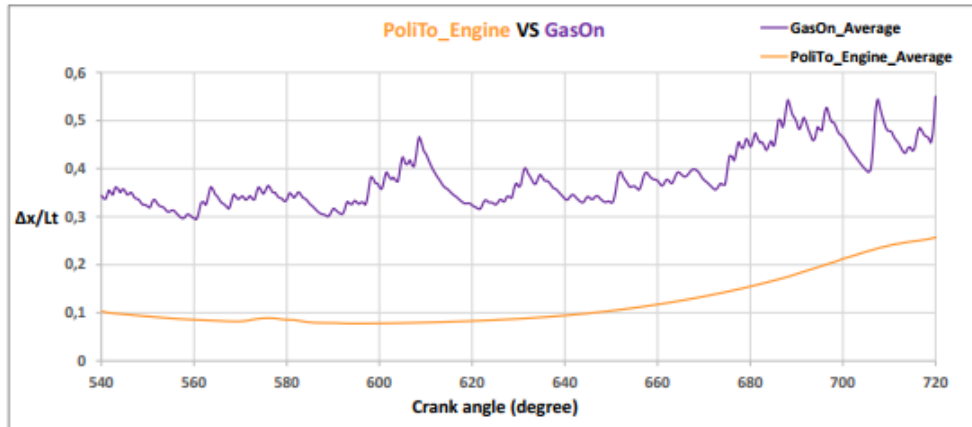
Ensembling (GasOn)





### Ensembling (Polito Engine VS GasOn)

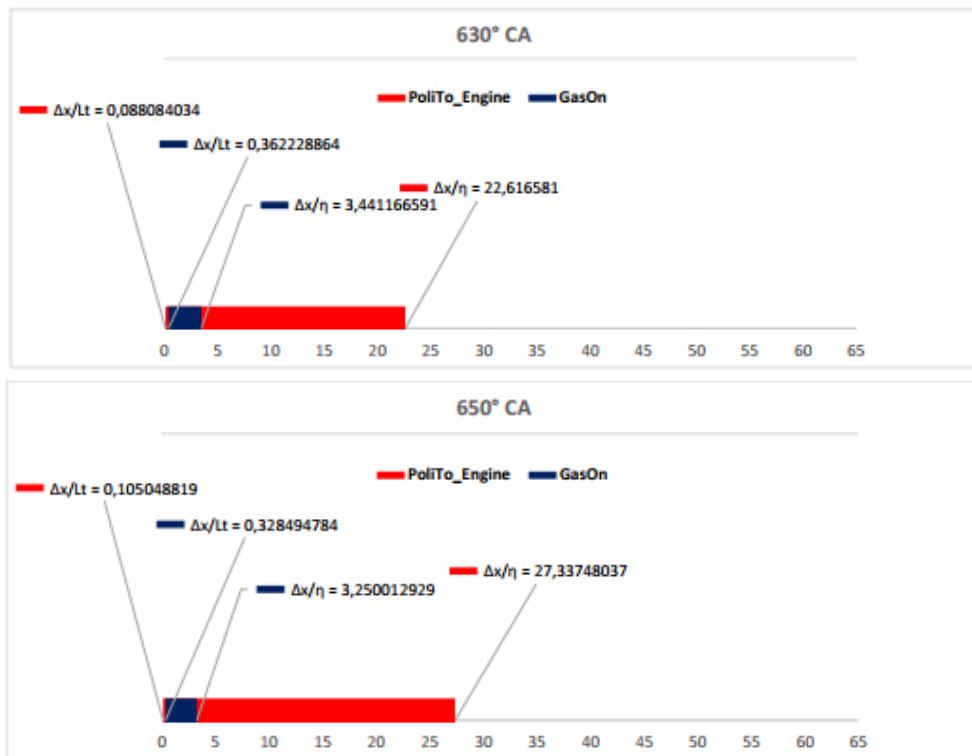


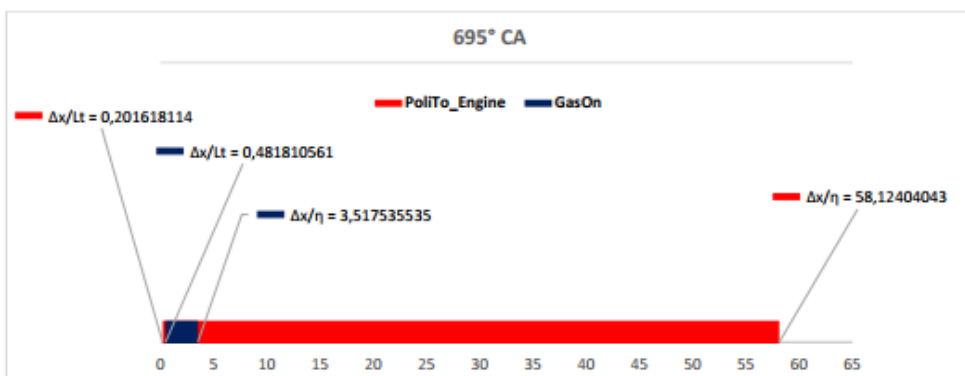
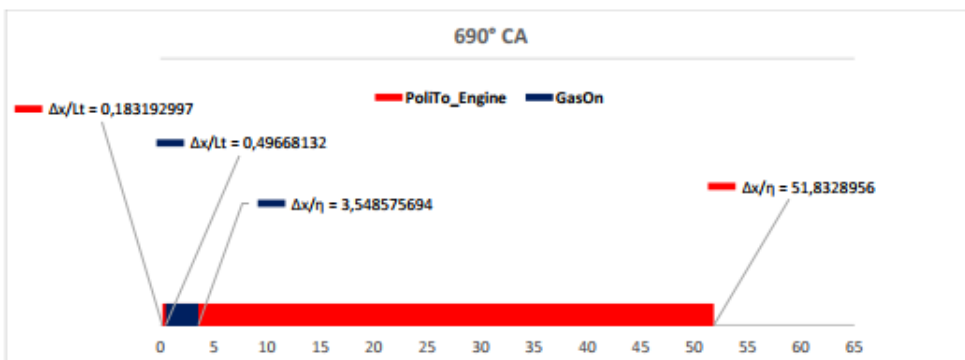
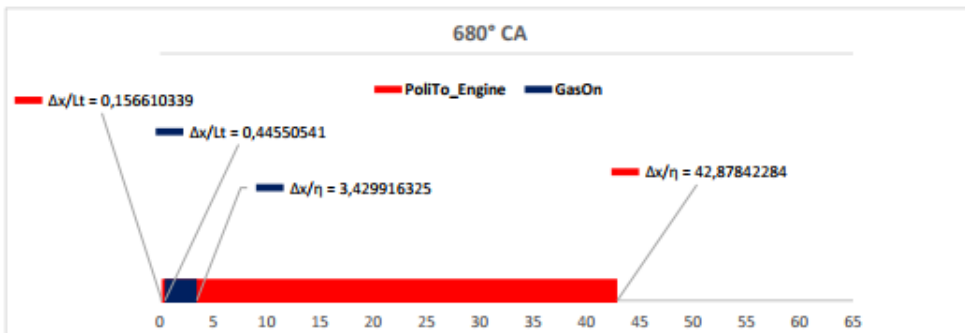
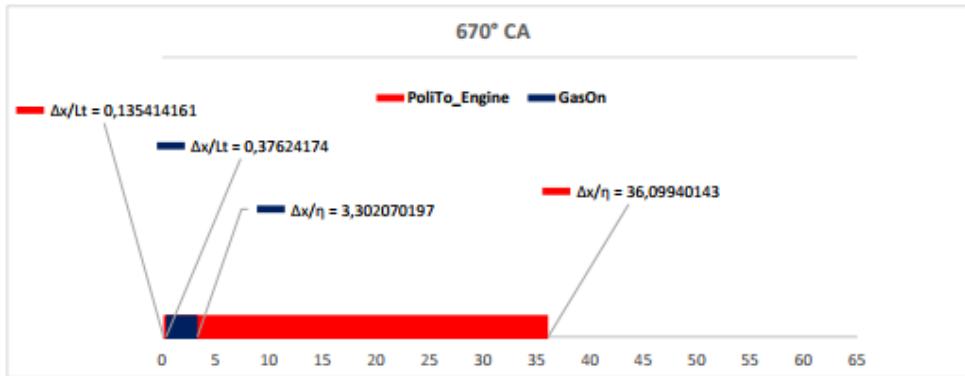


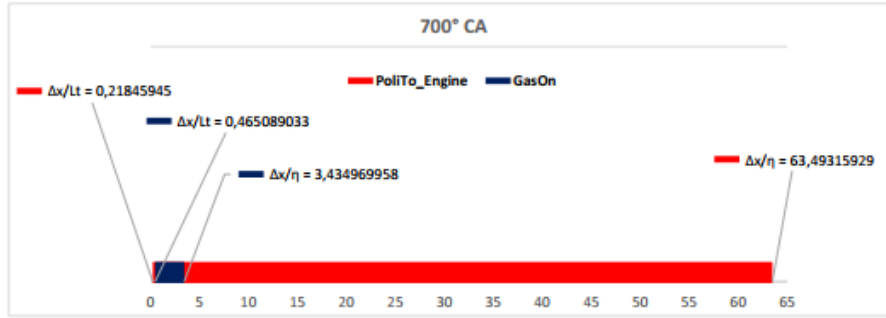
## 4.6 Mesh Independence

Through the latter section, we want to investigate whether our cell-size which is  $\delta x = 1\text{mm}$  is a proper choice or not.

To do so, for some specific crank angles which have been mentioned before, we apply Kolmogorov and integral length scale ratios of both Polito engine and GasOn on a same scale which let us have a clear comparison between them and realizing the range of eddies at a specific crank angle.







By referring to the Table 4.1, we observe that, For PoliTo Engine the length range of eddies vary between 0.044 (mm) and 11.364 (mm) which is much higher than GasOn range.

	<b>GasOn</b>	<b>Polito Engine</b>
$\frac{\Delta x}{\eta}$	3.441	22.617
$\frac{\Delta x}{L_t}$	0.3623	0.088
$\eta(mm)$	0.29	0.044
$L_t(mm)$	2.76	11.364

**Table 4.1:** 630° Crank angle degree (CAD)

## 4.7 Conclusion

We conclude that, the mesh size equal to 1 mm can be convenient for GasOn but in the case of PoliTo Engine we can even refer to coarse mesh size of my colleague's model ,which has been already implemented, that is  $\Delta x = 2$  (mm) and gives us the same result and also we can save the computational time. It is True that the best solution for PoliTo Engine is of setting the cell size  $\Delta x = 0.044$  (mm) as Kolmogorov scale, but is not an intelligent and efficient choice.



## Chapter 5

# Laminar Flame Speed

### 5.1 Laminar Premixed Flame

As the term “premixed” flame implies, this flame involves complete pre-mixing of the fuel and oxidizer prior to arrival at the flame zone. A common example of this type of flame is a Bunsen burner flame. A basic Bunsen burner device can be shown in the Figure below[6]. in a Bunsen burner device, nat-

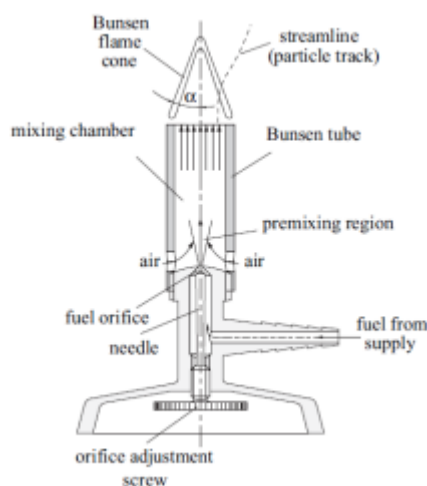


**Figure 5.1:** Schematic of Bunsen Burner[6]

ural gas enters through a control valve in the base of the burner. As the gas flows upward in the burner tube, air is inducted through slots near the base of the burner. The slots can be adjusted to control the amount of air induced into the burner tube relative to the gas flow. This controls the weight of the air-fuel mixture and finally lambda ( $\lambda$ ). The mixing chamber must be long enough to generate a premixed gas transferring from the Bunsen tube into the surroundings. The mixture of fuel gas and air flows out the top of the burner tube where it is stabilized to create the familiar blue flame cone of a Bunsen burner.

The kinematic balance of this process is illustrated for a steady oblique flame in Figure (5.2)[6]. The oncoming flow velocity vector  $\nu_u$  of the unburnt mixture (subscript u) is split into a component  $\nu_{n,u}$  which is tangential to the flame and into a component  $\nu_{n,u}$  normal to the flame front.

Due to thermal expansion within the flame front the normal velocity component is increased, since the mass flow density  $\rho\nu_n$  through the flame must be

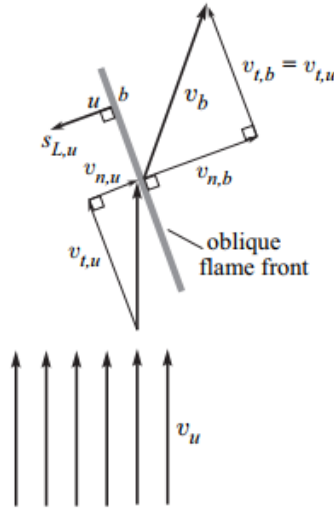


**Figure 5.2:** Kinematic balance for a steady oblique flame[6]

the same in the unburnt mixture and in the burnt gas (subscript b).

$$(\rho v_n)_u = (\rho v_n)_b \quad (5.1)$$

$$v_{n,b} = v_{n,u} \frac{\rho_u}{\rho_b} \quad (5.2)$$

The tangential velocity component  $v_t$  is not affected by the gas expansion and remains the same

$$v_{t,b} = v_{t,u} \quad (5.3)$$

Vector addition of the velocity components in the burnt gas in Figure 5.2 then leads to  $v_b$  which points into a direction which is deflected from the flow direction of the unburnt mixture. Finally, since the flame front is stationary in this experiment, the burning velocity  $S_{L,u}$  with respect to the unburnt mixture must be equal to the flow velocity of the unburnt mixture normal to the front.

$$S_{L,u} = v_{n,u} \quad (5.4)$$

With the Bunsen flame cone angle in Figure 5.2 denoted by  $\alpha$  the normal velocity is  $v_{n,u} = v_u \sin \alpha$  and it follows

$$S_{L,u} = v_u \sin \alpha \quad (5.5)$$

This allows to experimentally determine the burning velocity by measuring the cone angle  $\alpha$  under the condition that the flow velocity  $v_u$  is uniform across the tube exit. If this is not the case the flame angle also varies with radial distance, since the burning velocity  $S_{L,u}$  is essentially constant.

Another example for an experimental device to measure laminar burning velocities is the combustion bomb figure within which a flame is initiated by a central spark.

Spherical propagation of a flame then takes place which may optically be detected through quartz windows and the flame propagation velocity  $dr_f/dt$  may be recorded. Now the flame front is not stationary.

If the radial flow velocities are defined positive in inward direction, the velocity of the front must be subtracted from these in the mass flow balance through

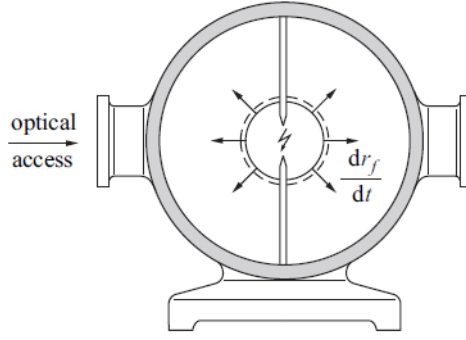


**Figure 5.3:** Laminar spherical flame propagation in a combustion bomb

the flame front

$$\rho_u \left( v_u - \frac{dr_f}{dt} \right) = \rho_b \left( v_b - \frac{dr_f}{dt} \right) \quad (5.6)$$

At the flame front the kinematic balance between propagation velocity, flow velocity and burning velocity with respect to the unburnt mixture is

$$\frac{dr_f}{dt} = v_u + S_{L,u} \quad (5.7)$$

Similarly, the kinematic balance with respect to the burnt gas is

$$\frac{dr_f}{dt} = v_b + S_{L,b} \quad (5.8)$$

In the present example the flow velocity  $v_b$  in the burnt gas behind the flame due to symmetry is zero. This leads with Eqs. (5.6) and (5.7) to

$$\frac{dr_f}{dt} = \frac{\rho_u}{\rho_u - \rho_b} v_u = v_u + S_{L,u} \quad (5.9)$$

This velocity is induced by the expansion of the gas behind the flame front. Furthermore it follows that the flame propagation velocity is related to the burning velocity  $S_{L,u}$  by

$$\frac{dr_f}{dt} = \frac{\rho_u}{\rho_b} S_{L,u} \quad (5.10)$$

Measuring the flame propagation velocity  $dr_f/dt$  then allows to determine  $s_{L,u}$ . Furthermore, from Eq. (5.8) it follows with  $v_b = 0$  that

$$dr_f/dt = s_{L,b} \quad (5.11)$$

The comparison of Eqs. 5.10 and 5.11 shows that the burning velocity with respect to the burnt gas is by a factor  $\frac{\rho_u}{\rho_b}$  larger than that with respect to the unburnt gas.

The model in figure 5.4[6] shows the flame structure of laminar lean flames. This model is a basic understanding of how flame interaction with unburned gases occurs. Firstly, the gases are heated in a preheat zone and then it reaches the inner layer or reaction zone. In reaction zone reactants converts to burned

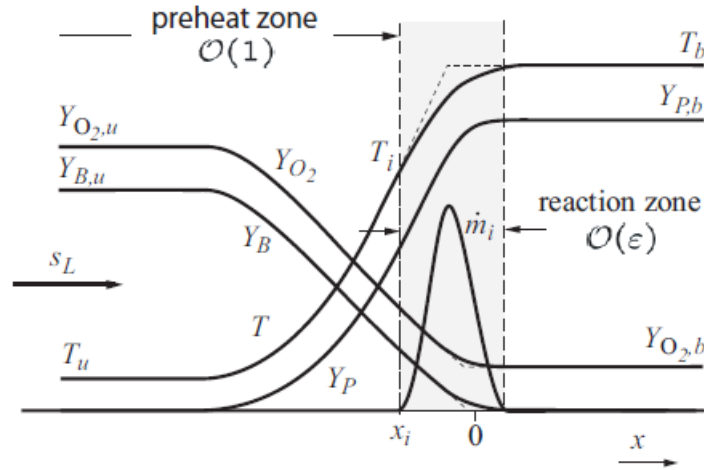


Figure 5.4: Flame structure of laminar lean flame [6]

gases which can be found in the oxidation layer (not mentioned in the figure - left most area). This model is important to understand the concept of flame thickness, when the flow becomes turbulent, the wrinkling of this zone affects the heat and mass transfer between the burned gases and unburned gases. For explanation of the model refer [6]. We will now consider the general case with multi-step chemical kinetics.

### 5.1.1 Governing equations

The fundamental property of a premixed flame, the burning velocity  $S_L$  may be calculated by solving the governing conservation equations for the overall mass, species and temperature.

Continuity

$$\frac{d(\rho u)}{dx} = 0 \quad (5.12)$$

Species

$$\rho u \frac{dY_i}{dx} = -\frac{dj_i}{dx} + \dot{m}_i \quad (5.13)$$

Energy

$$\rho u c_p \frac{dT}{dx} = \frac{d}{dx} \left( \lambda \frac{T}{dx} \right) - \sum_{i=0}^k h_i \dot{m}_i - \sum_{i=0}^k c_p j_i \frac{Dt}{dx} + \frac{\partial p}{\partial t} \quad (5.14)$$

The continuity equation may be integrated once to yield

$$\rho u = \rho_u S_L \quad (5.15)$$

The system of Eqs 5.12-5.15 may be solved numerically with the appropriate upstream boundary conditions for the mass fractions and the temperature and zero gradient boundary conditions downstream. Thus results in the Kinetic mechanism model which will be discussed later and which is used for the calculation of laminar flame speed in our project

As an example taken from [13] calculations of the burning velocity of premixed

methane-air flames using a mechanism that contains only C1-hydrocarbons and a mechanism that includes the C2-species are shown in Figure as a function of the equivalence ratio  $\phi$ . The two curves are compared with compilations of various data from the literature. It is seen that the calculations with the C2-mechanism shows a better agreement than the C1-mechanism.

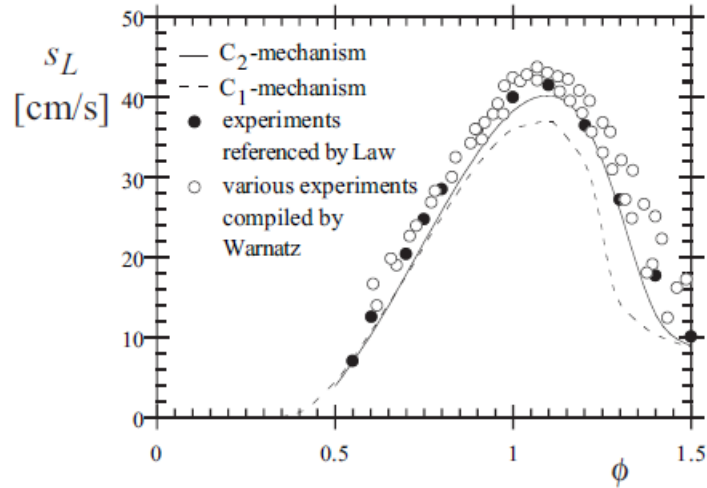


**Figure 5.5:** Burning velocities calculated with a starting C1-Mechanism and a starting C2-mechanism, several data compiled by Warnatz[14] and recent data referenced by Law[15] for atmospheric methane-air flames

## 5.2 Methods to predict Laminar flame speed

To develop the realistic prediction of laminar flame speed, generally 2 methods are used:

### 1. Power Laws

The laminar flamespeed can be calculated by one of three different approaches[10].

#### (a) Metghalchi and Keck

The laminar flamespeed can be calculated by one of three different approaches. The first method is to use the Metghalchi and Keck (1982) correlation, given by

$$S_{L_{ref}} = B_m + B_2(\phi - \phi_m)^2 \quad (5.16)$$

Where  $\phi$  is the equivalence ratio,  $B_m$ ,  $B_2$ , and  $\phi_m$  are user-supplied constants appropriate for the fuel and oxidizer used in the simulation.

#### (b) Gulder

The second method is to use the Gulder (1984) correlation, given by:

$$S_{L_{ref}} = \omega \phi^\eta \exp[-\zeta(\phi - 1.075)^2] \quad (5.17)$$

where  $\omega$ ,  $\phi$ , and  $\zeta$  are user-supplied constant appropriate for the fuel and oxidizer used in the simulation.

Once the reference laminar flamespeed is calculated at the reference pressure and temperature, the laminar flamespeed is adjusted for the actual pressure and temperature using the following equation:

$$S_L = S_{L_{ref}} \left( \frac{T_u}{T_{u_{ref}}} \right)^\gamma \left( \frac{P}{P_{ref}} \right)^\beta (1 - 2.1Y_{dil}) \quad (5.18)$$

Where  $T_u$  is the unburned temperature,  $T_{u_{ref}}$  is the reference unburned temperature,  $P$  is the pressure,  $P_{ref}$  is the reference pressure,  $Y_{dil}$  is the mass fraction of dilution species. The temperature and pressure exponents in Equation 5.14 are defined as:

$$\gamma = \gamma_{ref} - 0.8(\phi - 1) \quad (5.19)$$

and

$$\beta = \beta_{ref} + 0.22(\phi - 1) \quad (5.20)$$

### (c) user-supplied data tables

The third method for calculating the laminar flamespeed makes use of user-supplied data tables. These data tables must have the laminar flamespeed tabulated as a function of mixture fraction, temperature, pressure, and dilution fraction[10].

2. **Kinetic Mechanisms** Reaction mechanism are step by step descriptions of what occurs in a molecular level. It describes the transition state, also the order in which bonds form and break and the rate of each step. The reaction rate for each species are defines as per:

$$k_k = A_k T^{n_k} \exp\left(-\frac{E_k}{RT}\right) \quad (5.21)$$

Where  $K_k$  is rate coefficient,  $A_k$  is the frequency factor,  $n_k$  is the pre-exponential temperature exponent and  $E_k$  is the activation energy of reaction k.

Chemical kinetic mechanisms are defined for the different composition of fuel, also It depends on the number of species defined and the sub-reactions of each species. For example in a C1-C3 mechanism, the reaction of C3 species are involved.

## 5.3 Gulder vs LFS table

### 5.3.1 Reliability

In this practice, the target is to figure out how the different methods are reliable respect to each other. for this purpose according to Gulder correlation

and LFS table two separate models have been calibrated for pure methane as a fuel with consideration of different equivalence ration  $\lambda$  to see how they behave accordingly.

- **Pure Methane ( $\lambda = 1.4$ )**

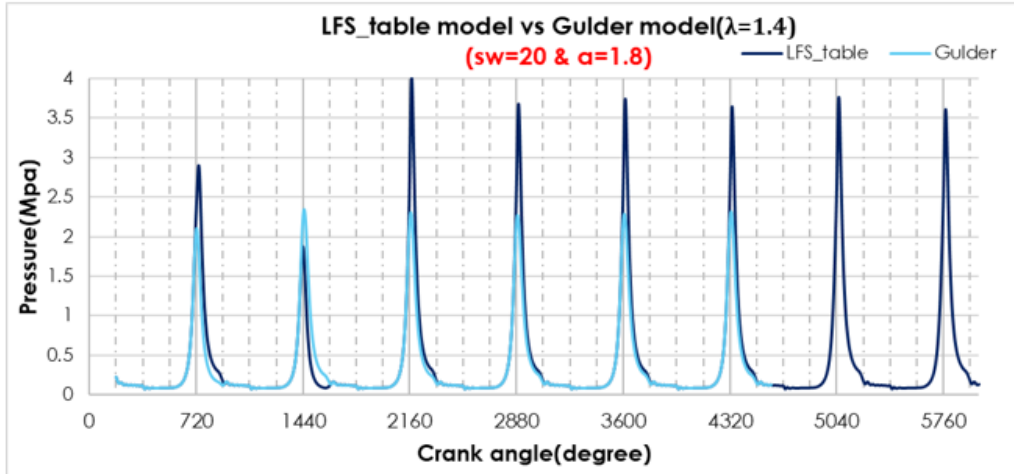


**Figure 5.6:** The base calibration for both models

The Figure 5.6 shows the starting attempt which implemented base on some parameters that directly affect the combustion phase which their values are alike for both starting models. those parameters are the spark advance degree (SAD), surface wrinkling factor, and ( $\alpha$ ) which is a constant for turbulent stretch.

Consistent high cycle to cycle variation is observable in Figure 5.5. for our purpose, we re-calibrated the Gulder model in order to achieve a proper convergence. This happened by trying different wrinkling factor and  $\alpha$ .

In order to utilize the time, we used (map files) in CONVERGE STUDIO which gives the possibility to work just on a specific cycle.

Case	$\alpha$	WF
LFStable (base)	1.8	20
Gulder (case1)	1.8	20
Gulder (case2)	2.1	20
Gulder (case3)	1.8	24

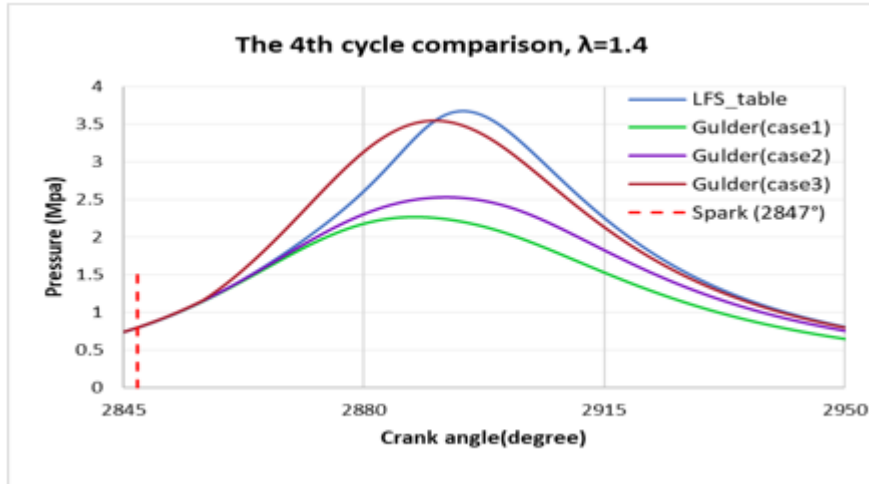


**Figure 5.7:** Gulder model re-calibration

By referring to Gulder(case3) For the 4th cycle a good approximation had been achieved, but once started from  $180^\circ$ , the effect of the factors damped down, so we were obliged to increase the values much more than what we expected.

Case	$\alpha$	WF
LFStable (base)	1.8	20
Gulder (case4*)	5.5	30
<b>Gulder (case5)</b>	<b>5.5</b>	<b>36</b>

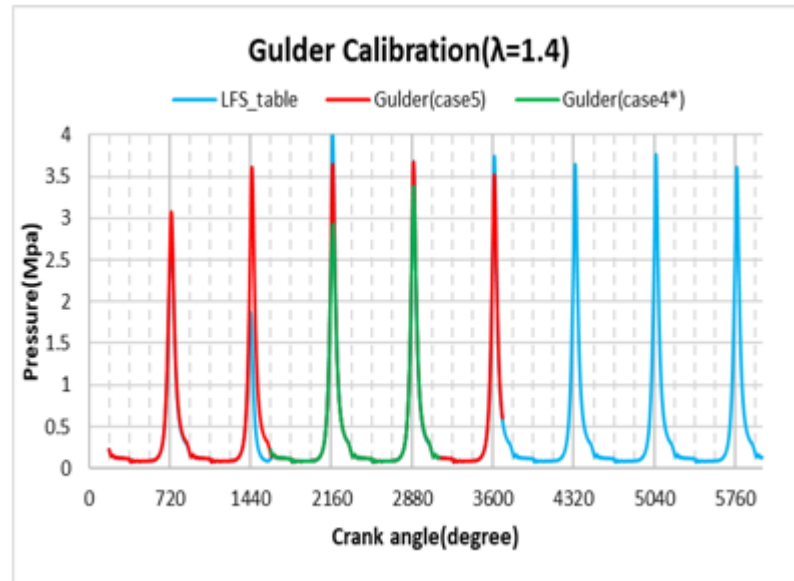


Figure 5.8: Gulder model re-calibration

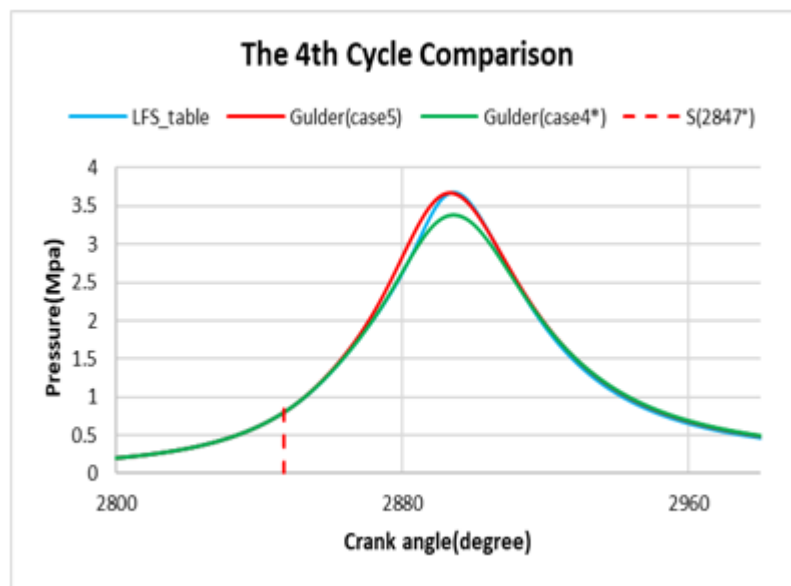


Figure 5.9: Gulder model re-calibration

Finally, by a notable change in  $\alpha$ , an acceptable convergence has been achieved. (Figure 5.8)

- **Pure Methane** ( $\lambda = 1.0$ )

According to our purpose, the two models still should be compared for  $\lambda = 1.0$  which, of course, the calibrated parameters should be altered accordingly. the base case for both models has been calibrated with  $\alpha$  and WF equal to 1.7 and 15 respectively.

Again a consistent unacceptable cycle to cycle variation has been achieved which obliged us to re-calibrate the Gulder model.

Case	$\alpha$	WF
LFStable (base)	1.7	15
Gulder	2.5	13

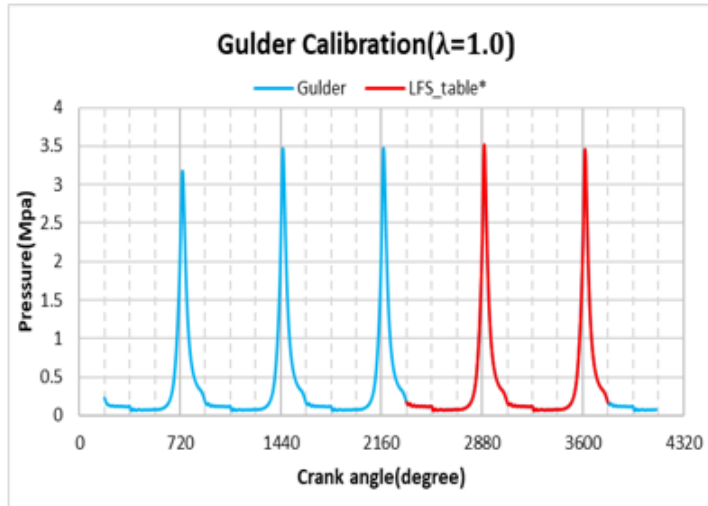


Figure 5.10: Gulder model re-calibration

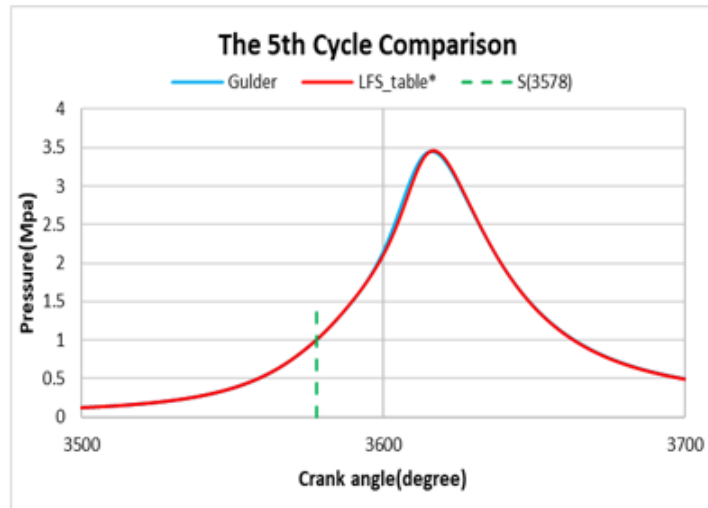


Figure 5.11: Gulder model re-calibration

### 5.3.2 Conclusion

Based on our investigation, we can conclude, using the table to calculate laminar flame speed doesn't eliminate the need of re-calibration ( from  $\lambda = 1.0$  to  $\lambda = 1.4$ ) which is observable from the figures and tables where  $\alpha$  varies from 1.7 to 1.8 which is still close to literature indications, it says the fact that even if we don't have the experimental result we can suppose a predictive variation of  $\alpha$ . while a wh have seen a notable change of  $\alpha$  for Gulder model, actually

more than doubled from  $\lambda = 1.0$  to  $\lambda = 1.4$ .

Of all, we can conclude the Gulder correlation isn't reliable and predictive.

## 5.4 The Effect of EGR on Gulder and LFStable Models

### 5.4.1 Introduction to Exhaust Gas Recirculation (EGR)

This is a technology which is used in automobile engines to reduce pollution, specifically the amount of nitrogen oxides ( $NO_x$ ) which are getting emitted into the atmosphere.

#### What EGR does?

It recirculates a portion of exhaust gas to the combustion chamber. actually, by supplying inert gas (*is a gas which doesn't undergo chemical reactions under a set of given condition*) like carbon dioxide ( $CO_2$ ) which acts as an absorbent and reduces the combustion heat, so the peak temperature in cylinder gets reduced, therefore the chance of creation of  $NO_x$  reduces.

In fact, nitrogen oxide ( $NO_x$ ) is formed when nitrogen ( $N_2$ ) and oxygen ( $O_2$ ) being combined together at high temperature. So by reducing heat inside the cylinder the chance of combination of  $N_2$  and  $O_2$  reduces so the production of  $NO_x$  gets reduced, but by the reduction in heat, the engine efficiency decreases a bit.

Let's see how the system works:

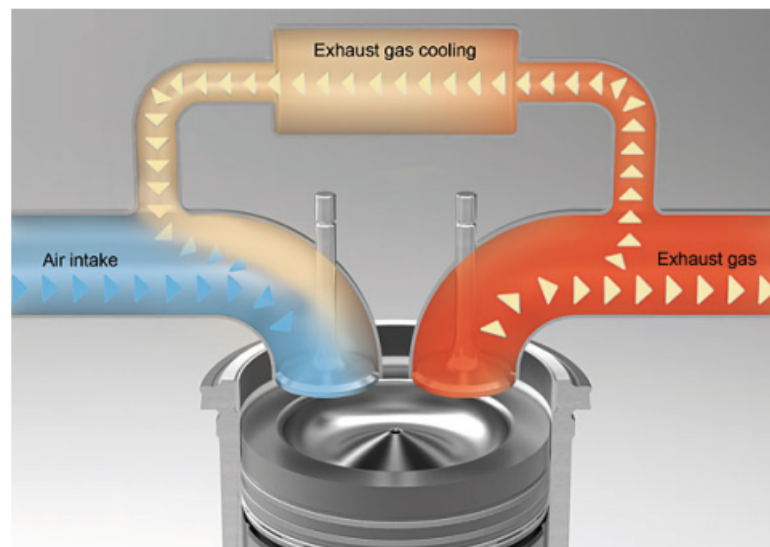


Figure 5.12: Exhaust gas recirculation[7]

When the engine works, it requests air and as we have already discussed its major components are  $O_2$  and  $N_2$  with roughly 21% and 79% respectively.

The air is sucked into input manifold toward cylinder, then inside the cylinder compression and combustion takes place and what happens that  $O_2$  and  $N_2$  decomposed and  $NO_x$  is created.

$NO_x$  is a very harmful product, and what we want is to reduce it as much as possible. one possible way is to reduce the temperature inside the combustion

chamber.

As we see in the Figure 5.12, some portions of exhaust gas pass through EGR coolant and then, when the fuel gets mixed with cool exhaust gas, the combustion takes place cooler which finally leads to decrease the chance of  $NO_x$  production.

But should be noticed, EGR technique also reduces the in-cylinder peak pressure Figure 5.13 which leads to a decrement of the engine performance, so a proper trade-off should be adopted.

Finally EGR technique reduces the  $NO_x$  production and also gives the advantage of Imparting knock resistance in SI engines.

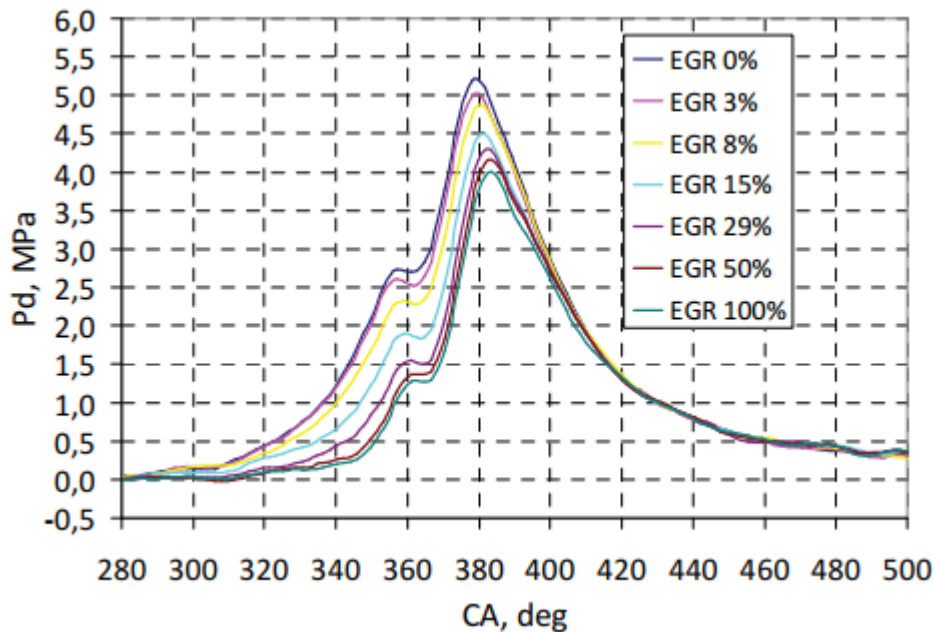


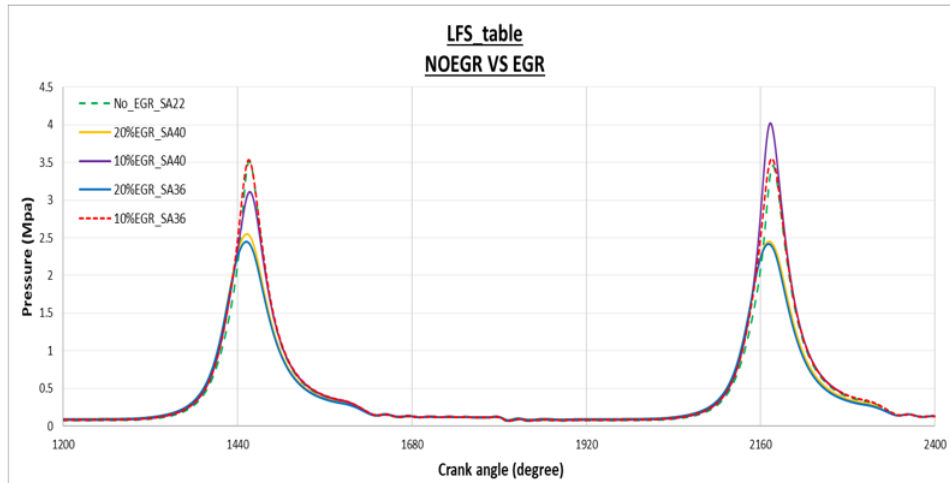
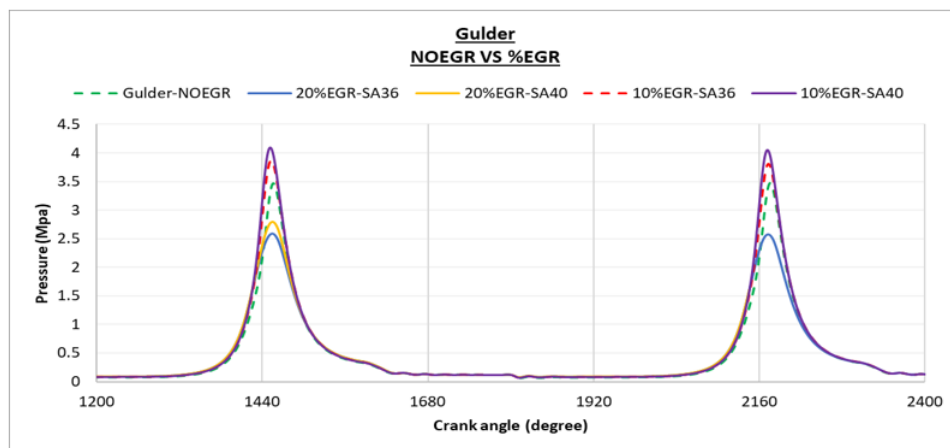
**Figure 5.13:** Differential pressure at different EGR valve opening level (1600rpm, 190 Nm)[16]

## 5.4.2 Procedure

### EGR effect on Gulder and LFStable models

In this step we are going to investigate the effect of EGR on Gulder and LFStable models which we have already worked on them. Actually comparing for each model the NO EGR case which has been already calibrated with its EGR cases. As before this time also we consider pure methane as a fuel base on the equivalence ratio equal ( $\lambda$ ) to 1.0.

Due to the effect of EGR which damps down the peak pressure, by advancing the ignition time (spark), there would be the possibility of recovery.

Figure 5.14: LFStable model  $\lambda = 1.0$ Figure 5.15: Gulder model model  $\lambda = 1.0$ 

### 5.4.3 Conclusion

More, specifically, from the previous section, we got a perfect convergence of the models but the point was the significant change in the  $\alpha$  parameter for Gulder model. then we fixed the values of the parameters (convergence has been achieved by), then in this step of our analysis we applied 10% and 20% of EGR to both models with advancing the ignition time by some degree, for LFStable model we have got a proper convergence while we applied the same EGR and ignition time but we can observe the failure of Gulder model to achieve the convergence.



## Chapter 6

# Use of Hydrogen-Methane Blends in Internal Combustion Engines

### 6.1 Introduction

Traditionally, to improve the lean-burn capability and flame burning velocity of natural gas engines under lean-burn conditions, an increase in flow intensity is introduced in the cylinder, and this measure always increases the heat loss to the cylinder wall and increases the combustion temperature as well as the NO<sub>x</sub> emission.

One effective method to solve the problem of the slow burning velocity of natural gas is to mix natural gas with fuel that possesses fast burning velocity. Hydrogen is regarded as the best gaseous candidate for natural gas due to its very fast burning velocity, and this combination is expected to improve lean-burn characteristics and decrease engine emissions. The hydrogen blends in CNG can range from 5 to 30% by volume. Hythane is a 15% blend of hydrogen in CNG by energy content, which was patented by Frank Lynch of Hydrogen Components Inc, USA. A typical 20% blend of hydrogen by volume in CNG is 3% by mass or 7% by energy[1].

An overall comparison of the properties of hydrogen, CNG, and 5% HCNG blend by energy and gasoline is given in Table 6.1. It is to be noted that the properties of HCNG lie in between those of hydrogen and CNG[2].

Prperties	$H_2$	CNG	HCNG	Gasoline
Stoichiometric volume fraction in air,(vol %)	29.53	9.43	22.8	1.76
Limits of flammability in air,(vol %)	4-75	5-15	5-35	1.0-7.6
Auto ignition temp. K	858	813	825	501-744
Flame temp in air K	2318	2148	2210	2470
Maximum energy for ignition in air, MJ	0.02	0.29	0.21	0.24
Burning velocity in NTP air, cm s <sup>-1</sup>	325	45	110	37-43
Quenching gap in NTP air, cm	0.064	0.203	0.152	0.2
Diffusivity in air cm <sup>2</sup> s <sup>-1</sup>	0.63	0.2	0.31	0.08
Percentage of thermal energy radiated	17-25	23-33	20-28	30-42
Normalized flame emissivity	1.0	1.7	1.5	1.7
Equivalence ratio	0.1-7.1	0.7-4	0.5-5.4	0.7-3.8

**Table 6.1:** Overall comparison of properties of hydrogen, CNG, HCNG and gasoline[2]

Hydrogen also has a very low energy density per unit volume and as a result, the volumetric heating value of the HCNG mixture decreases Table 6.2 as the proportion of hydrogen is increased in the mixture.

Properties	CNG	HCNG 10	HCNG 20	HCNG 30
$H_2$ [vol %]	0	10	20	30
$H_2$ [mass %]	0	1.21	2.69	4.52
$H_2$ [energy %]	0	3.09	6.68	10.94
LHV [MJkg <sup>-1</sup> ]	46.28	47.17	48.26	49.61
LHV [MJNm <sup>-3</sup> ]	37.16	34.50	31.85	29.20
LHV stoichiometric mixture [MJNm <sup>-3</sup> ]	3.376	3.368	3.359	3.349

**Table 6.2:** Properties of CNG and HCNG blends with different hydrogen content[3]

Many researchers have studied the effect of the addition of hydrogen to natural gas on performances and emissions in the past few years[40-65].

As an example we can refer to Karim et al.[4]theoretically studied the addition of hydrogen on methane combustion characteristics at different spark timings. The theoretical results showed that the addition of hydrogen to natural gas could decrease the ignition delay and combustion duration at the same equivalence ratio. It indicated that the addition of hydrogen could increase the flame propagation speed, thus stabilizing the combustion process, especially the lean combustion process.

also, Ilbas et al. [5] experimentally studied the laminar burning velocities of hydrogen-air and hydrogen-methane-air mixtures. They concluded that increasing the hydrogen percentage in the hydrogen-methane mixture brought about an increase in the resultant burning velocity and caused a widening of the flammability limit Figure.

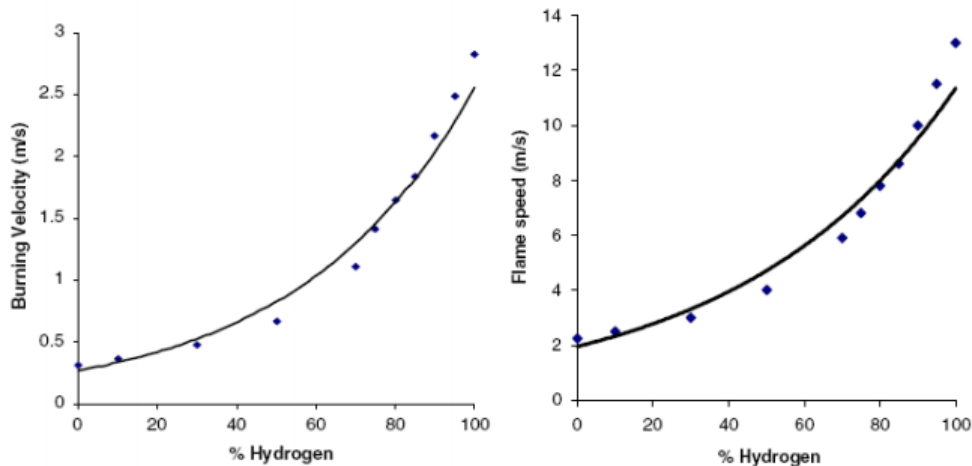


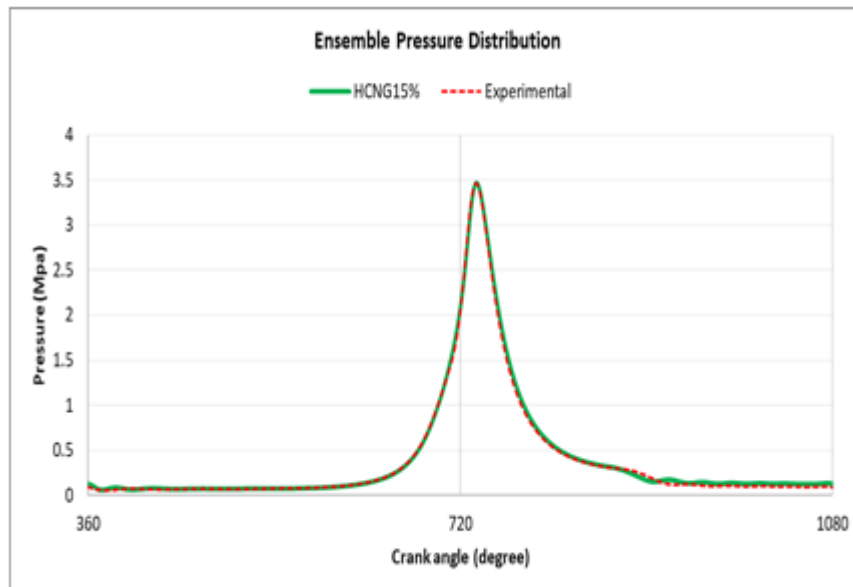
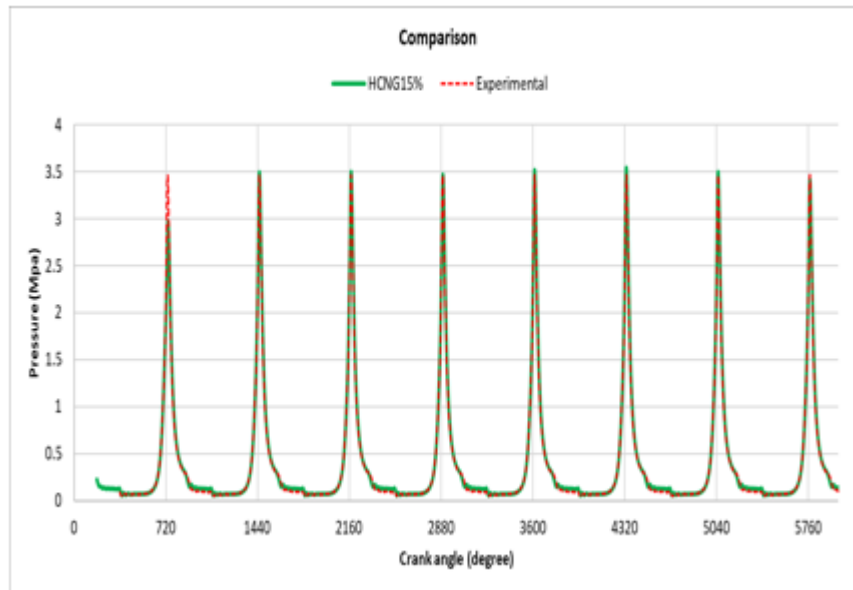
**Figure 6.1:** Burning velocities and flame speed for different percentages of hydrogen in methane ( $\phi = 1.0$ )[5]

## 6.2 Procedure

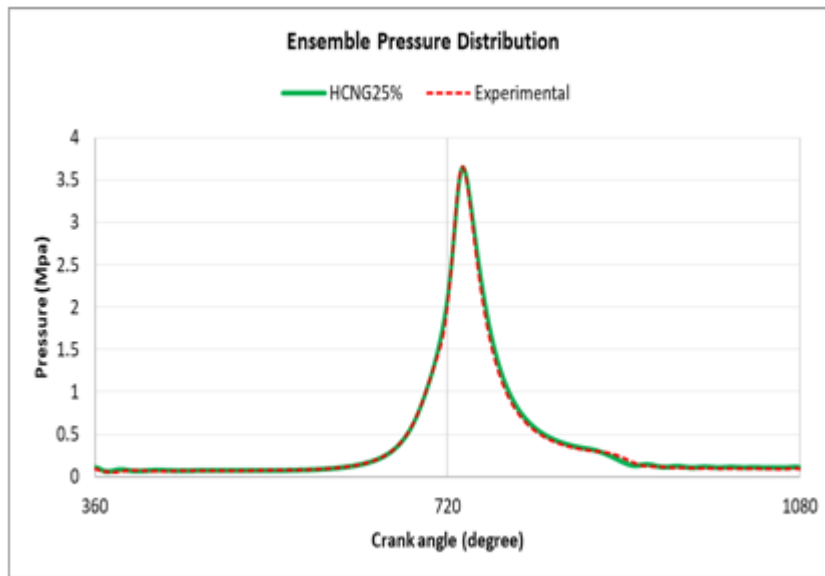
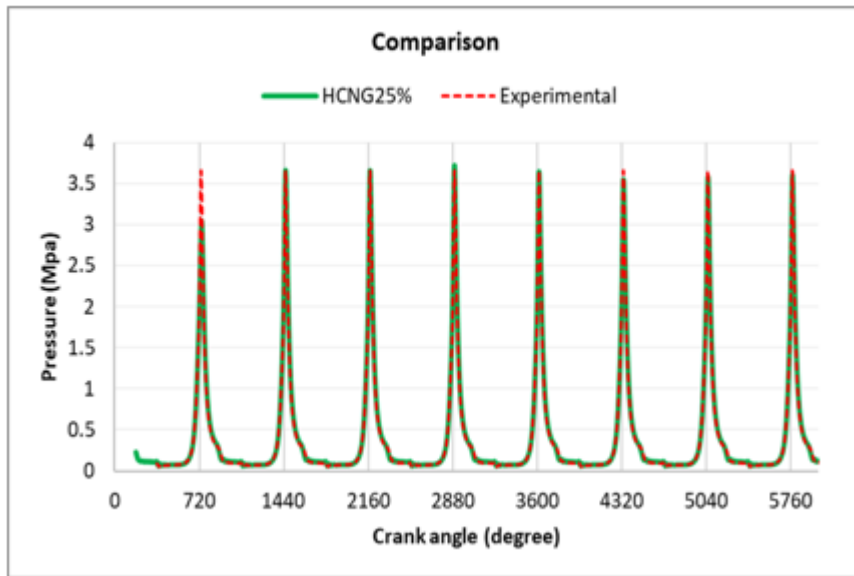
In this section we planned to investigate the effect of hydrogen on LFStable model.

To this purpose, 15% and 25% of hydrogen considered to be blended, for both  $\lambda = 1.0$  and  $\lambda = 1.4$  case. To this purpose, we got the LFS-table cases for  $\lambda = 1.0$  and  $\lambda = 1.4$  and new boundary condition applied accordingly to inlet and outflow( pressure and temperature). Also, a new ignition time and flame speed table for HCNG15 and HCNG25 has been adopted and finally we go to compare them with the experimental data.

### HCNG15% $\lambda = 1.0$



HCNG25%  $\lambda = 1.0$



By the first try We have got a great convergence for both HCNG15% and HCNG25% cases which is so interesting. actually no re-calibration needed. Now we want to implement the same investigation for both cases base on  $\lambda = 1.4$

HCNG15%  $\lambda = 1.4$

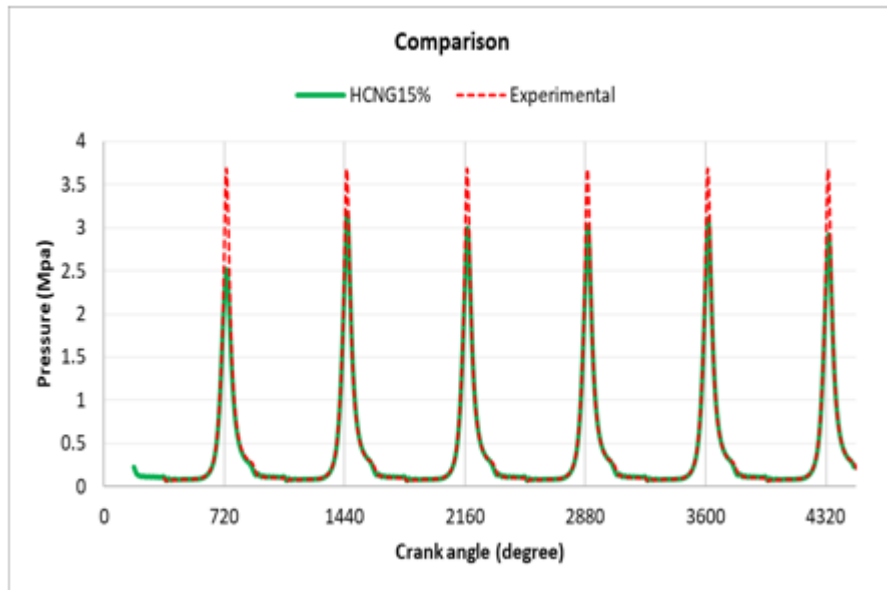


Figure 6.2: Wrinkling factor=20  $\alpha=1.8$

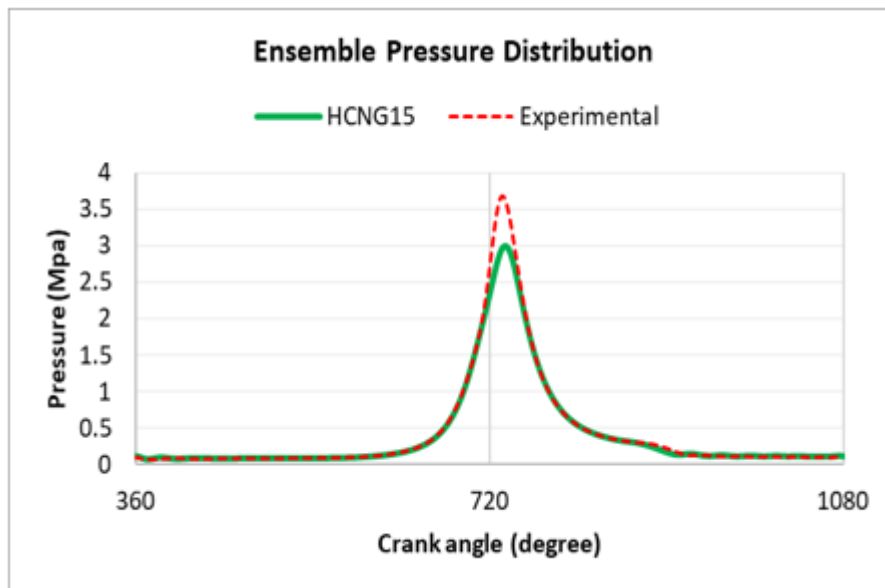
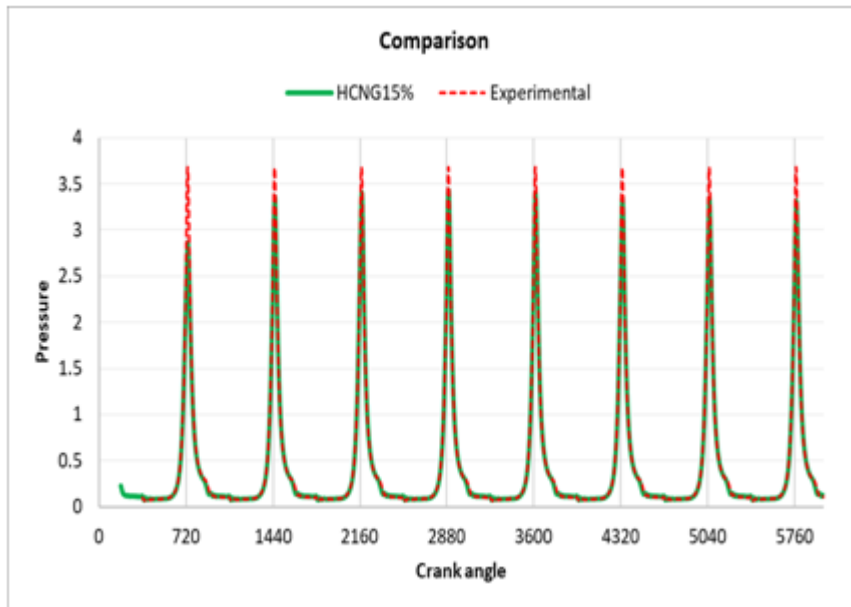
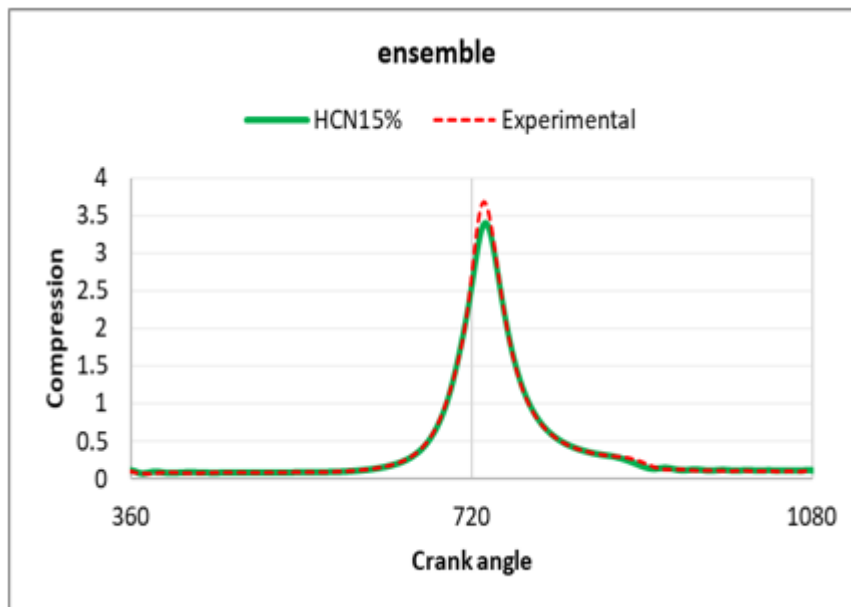


Figure 6.3: Wrinkling factor=20  $\alpha=1.8$

What is observed here by the Figures 6.2 and 6.3 is different than what we expected to see. There is a consistent high cycle to cycle variation, more than 5 bar which is out of the tolerance.

It means re-calibration needs by changing the wrinkling factor or  $\alpha$ .

Re-calibration HCNG15%  $\lambda = 1.4$ Figure 6.4: Wrinkling factor=30  $\alpha=1.8$ Figure 6.5: Wrinkling factor=30  $\alpha=1.8$ 

From the ensemble pressure distribution Figure 6.5, a convergence with an acceptable tolerance has been achieved. In re-calibration the wrinkling factor has been increased from 20 to 30.

Let's implement the same for HCNG25%.

HCNG25%  $\lambda = 1.4$

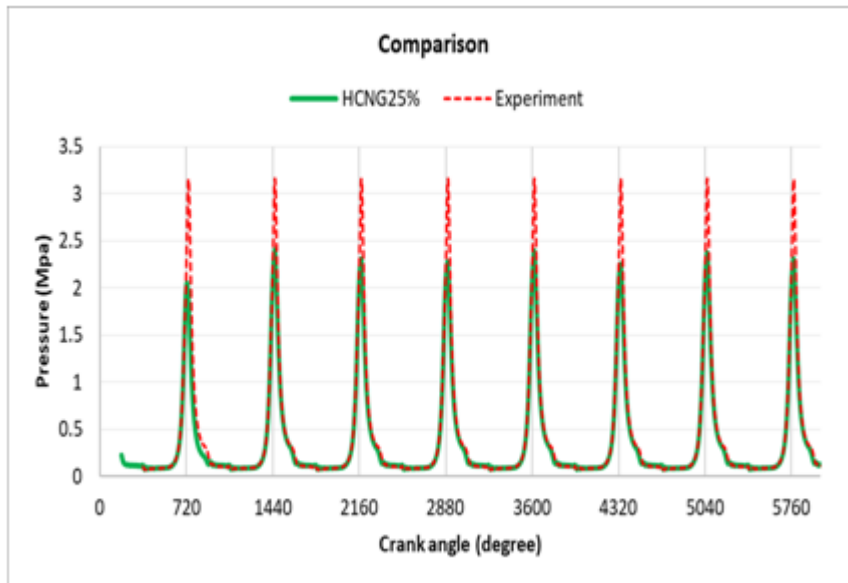


Figure 6.6: Wrinkling factor=20  $\alpha=1.8$

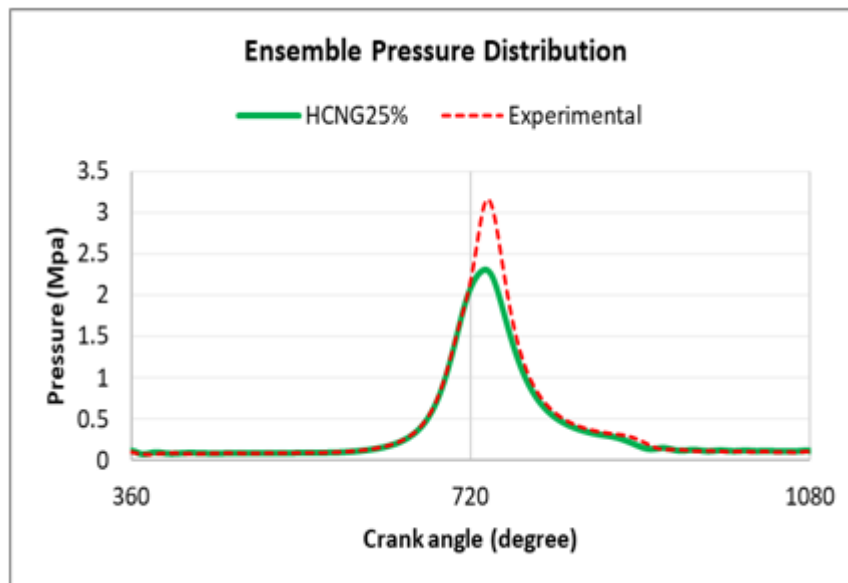
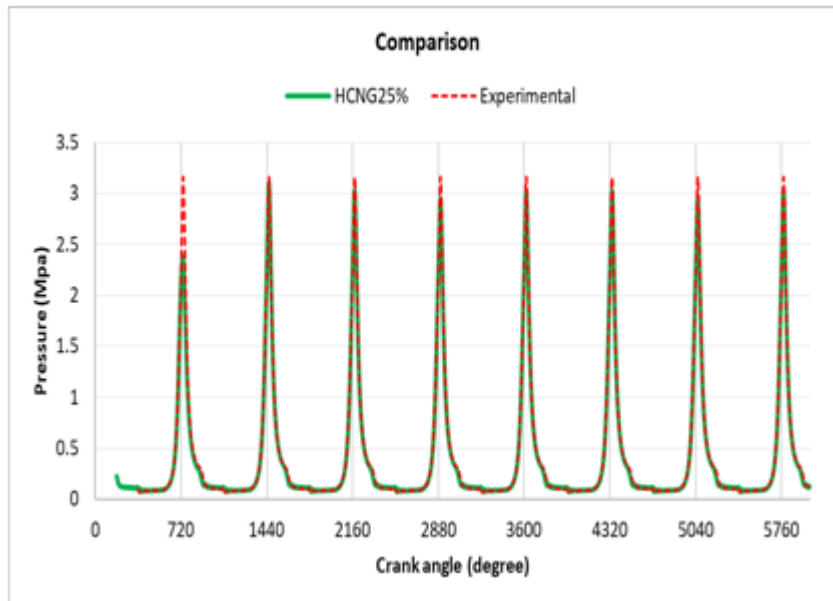
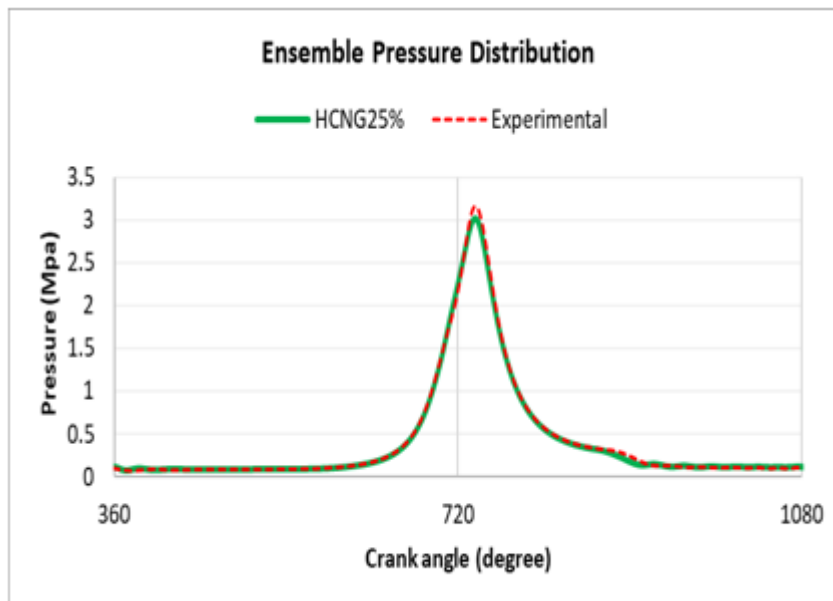


Figure 6.7: Wrinkling factor=20  $\alpha=1.8$

Again we observe non-convergent behavior from the models. so re-calibration needed.

Re-calibration HCNG25%  $\lambda = 1.4$ Figure 6.8: Wrinkling factor=35  $\alpha=2.1$ Figure 6.9: Wrinkling factor=35  $\alpha=2.1$ 

We have got a common point for lean mixture  $\lambda = 1.4$  where for both cases HCNG15% HCNG25%, re-calibration needed, while in contrary, no-calibration needed for  $\lambda = 1.0$ .

# Bibliography

- [1] Bilge Albayrak Çeper, "Use of Hydrogen-Methane Blends in Internal Combustion Engines," Erciyes University Faculty of Eng., Dept. of Mech Eng., Kayseri, Turkey
- [2] Patil K.R., Khanwalkar P.M., Thipse S.S., Kavathekar K.P., Rairikar S.D., Development of HCNG Blended Fuel Engine with Control of NO<sub>x</sub> Emissions, International Journal of Computer Information Systems and Industrial Management Applications (IJCISIM), ISSN: 2150-7988, 2010;2:087-095
- [3] Bell, S.R., Gupta, M., Extension of a Lean Operating Limit for Natural Gas Fuelling of a Spark Ignition Engine Using Hydrogen Blending., Combustion Sciences and Technology, 1997;123: 1-6, 23-48
- [4] Karim G.A., Wierzbka I., Al-Alousi Y., Methane-hydrogen mixtures as fuels. International Journal of Hydrogen Energy 1996;21(7):625-31.
- [5] Ilbas M., Crayford A.P., Yilmaz I., Bowen P.J., Syred N., Laminar-burning velocities of hydrogen-air and hydrogen-methane-air mixtures: An experimental study, Int J Hydrogen Energy 31;2006:1768 - 1779
- [6] Combustion theory, CEFRC summer school Princeton, N.Peters, RWTH Aachen
- [7] Dr. Johannes Kech, "How does Exhaust Gas Recirculation work?,"
- [8] RC Flagan - 1988, "Combustion Fundamentals,"
- [9] wikimedia.org, "Ideal-stoichiometry.jpg,"
- [10] Converge CFD Software Manual, 2016
- [11] Nate Laurell, "Natural Gas Overview,"(June 12, 2014)
- [12] x-engineer.org Engineering Tutorials, "Air-fuel ratio, lambda and engine performance,"
- [13] F. Mauss and N. Peters. Reduced kinetic mechanisms for premixed methane-air flames, in Reduced kinetic mechanisms for applications in combustion systems. Lecture Notes in Physics, Springer-Verlag Berlin, 75:58, 1993
- [14] [13] J. Warnatz. Comb. Inst., 384:369, 1981
- [15] C. K. Law. Compilation of recent experimental data of premixed laminar flames. Lecture Notes in Physics, Springer-Verlag Berlin, 30:19, 1993.

- [16] BIENIEK, A., MAMALA, J., GRABA, M., HENNEK, K. Impact of EGR control at in-cylinder pressure and ecological properties of CI off-road vehicle engine. *Combustion Engines*. 2017, 170(3), 88-95. DOI: 10.19206/CE-2017-314
- [17] Benoit Cushman-Roisin Thayer School of Engineering Dartmouth College, "Kolmogorov's Theory of Inertial Turbulence,"
- [18] André Bakker (2002-2005), "Kolmogorov's Theory,"